Historic Surface Faulting and Paleoseismicity in the Area of the 1954 Rainbow Mountain–Stillwater Earthquake Sequence, Central Nevada

by S. John Caskey, John W. Bell, Alan R. Ramelli, and Steven G. Wesnousky

Abstract   The Rainbow Mountain area was the site of three surface-rupturing earthquakes on 6 July and 23 August 1954. More than 50 field measurements of surface offsets constrain the distribution of slip along the discontinuous and distributed rupture zone that formed during the earthquake sequence. Vertical offsets reach a maximum of ~0.8 m with the average vertical offset being ~0.2 m. In contrast to original reports, we see evidence for a right-lateral component of slip along portions of the rupture zone, including offset stream channels (0.5–1.0 m), left-stepping *en echelon* scarps, and a well-preserved, 100-m-long mole track. The right-slip component is consistent with focal plane solutions for the events and recent geodetic results. Previously unmapped surface ruptures now extend the known rupture length of the sequence by 25 km to a total of 70 km. Surface ruptures along the previously unmapped Fourmile Flat fault are subparallel to and form a 10-km left step to the southeast of the Rainbow Mountain fault. Event locations and anecdotal information indicate that the Fourmile Flat ruptures represent minor, primary surface rupture associated with the large 6 July aftershock, triggered ~11 hr after the initial 6 July Rainbow Mountain event.

The paleoseismic histories of the Rainbow Mountain and Fourmile Flat faults, as recorded in natural and trench exposures, are different although both faults experienced three post ~15-ka surface rupturing events, including 1954. Bracketing ages for triultimate events on both faults do not overlap. However, constraints on the penultimate event for the Rainbow Mountain and triultimate event for the Fourmile Flat fault do overlap slightly, allowing the possibility that they may have ruptured close in time as in 1954. The Holocene slip rate for the Fourmile Flat fault (0.40 mm/yr) is similar to the post-latest Pleistocene rate for the Rainbow Mountain fault (0.20–0.46 mm/yr) even though the total length of the Fourmile flat (10 km) is much shorter than the overall length of the Rainbow Mountain rupture zone (~60 km), indicating that even minor faults can be important for assessing regional strain rates and patterns.

Introduction

The 1954 Rainbow Mountain–Stillwater earthquake sequence consisted of three moderate to large earthquakes that occurred within the Basin and Range province, approximately 20 km east of Fallon, Nevada (Fig. 1). The initial 6 July M_s 6.3 Rainbow Mountain earthquake was followed ~11 hr later by a large M 6.4 triggered event, herein referred to as the Fourmile Flat earthquake, and then 49 days later by the 23 August M_s 7.0 Stillwater earthquake (Fig. 1). The three earthquakes combined to produce a discontinuous north-trending zone of surface ruptures 70 km long and up to 12 km wide. The most prominent ruptures occurred along the Rainbow Mountain fault, which bounds the eastern escarpment of Rainbow Mountain, a moderately west-tilted

block of Miocene volcanic and sedimentary rocks (Stewart and Carlson, 1978).

The Rainbow Mountain–Stillwater sequence is the first of a more extensive 1954 earthquake sequence that also includes the 16 December M_s 7.2 Fairview Peak and M_s 6.8 Dixie Valley earthquakes to the east (Fig. 1). The 1954 sequence together with the 1915 M_s 7.6 Pleasant Valley and 1932 M_s 7.2 Cedar Mountain earthquakes to the north and south, respectively, define the central Nevada seismic belt (Fig. 1) (Wallace, 1984). The Rainbow Mountain–Stillwater sequence and the Fairview Peak earthquake produced right-normal-oblique motion on dipping faults (Doser, 1986; Fig. 1). These four right-oblique earthquakes are located in
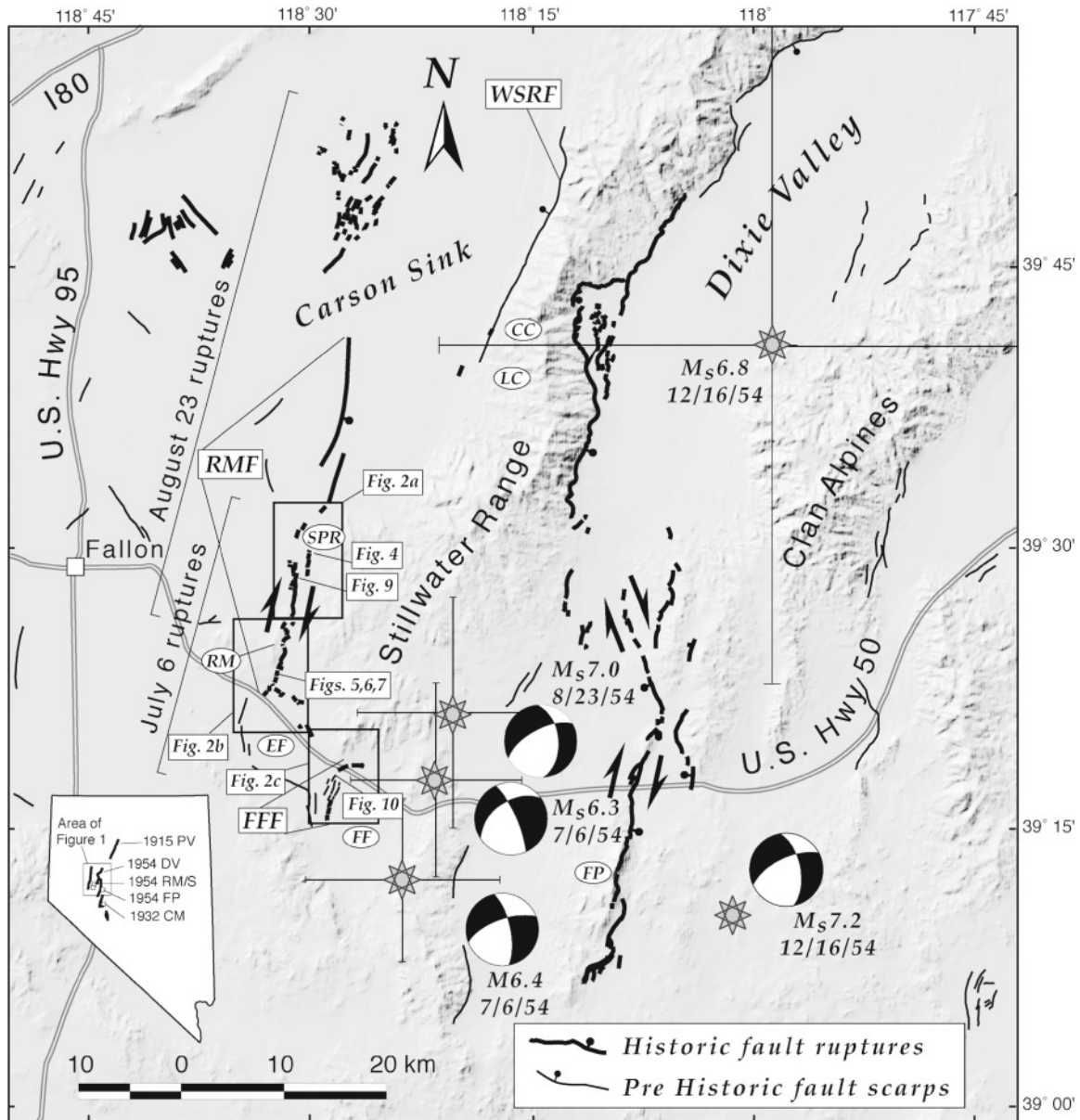
1255

Figure 1.   Location map for rupture zones of the 6 July and 23 August Rainbow Mountain–Stillwater and 16 December 1954 Fairview Peak and Dixie Valley earthquake sequence. Bar and ball on the down-thrown side of faults. Focal mechanisms and locations (stars with associated location uncertainty bars) are from Doser (1986). Fairview Peak and Dixie Valley rupture zones adapted from Caskey *et al.* (1996). Prehistoric faults are from Bell (1984) and Dohrenwend *et al.* (1996). Inset map shows locations and generalized rupture zones associated with the 1915 Pleasant Valley (PV), 1932 Cedar Mountain (CM), and 1954 Fairview Peak (FP), Dixie Valley (DV), and Rainbow Mountain–Stillwater (RM/S) earthquakes. Abbreviations: Fault names (large boxes): FFF, Fourmile Flat fault; RMF, Rainbow Mountain fault; WSRF, Western Stillwater Range fault. Place names (ovals): CC, Cox Canyon; EF, Eightmile Flat; FF, Fourmile Flat; FP, Fairview Peak; LC, Lambing Canyon; RM, Rainbow Mountain; SPR, Stillwater Point Reservoir. Other boxes denote locations of figures in text.

a transition zone between dominantly right-lateral earthquakes to the south (e.g., the 1872 Owens Valley and 1932 Cedar Mountain earthquakes) (Gianella and Callaghan, 1934; Beanland and Clark, 1994; Bell *et al.*, 1999) that occurred within the northwest-trending Walker Lane belt (Stewart, 1988), and predominantly normal dip-slip earthquakes to the north (e.g., the 1915 Pleasant Valley and 1954 Dixie Valley earthquakes) (Slemmons, 1957; Wallace, 1984; Caskey *et al.*, 1996), where the Basin and Range exhibits consistent north- to northeast-trending structural patterns.

Tocher (1956) originally reported on the general geological characteristics of the 1954 Rainbow Mountain–Stillwater earthquake sequence, and Steinbrugge and Moran (1956) reported on damage caused in the Fallon area. Tocher's field study was initiated immediately following the 6 July earthquake, so he was able to discriminate between the 6 July and 23 August rupture traces, which partially overlap along the Rainbow Mountain fault (Fig. 1). Tocher (1956) published 1:76,000-scale fault rupture maps that showed only about a 20-km-long portion of the rupture zone and included about a dozen measurements of surface offset. Slemmons (1957) later published a 1:250,000-scale compilation of the entire July–December 1954 rupture zones, which included additional rupture traces not shown on Tocher's (1956) original maps. Slemmon's compilation extended the mapped zone of the July–August rupture zone approximately 40 km northward into the Carson Sink. Bell's (1984) 1:250,000-scale fault compilation extended the zone of ruptures approximately 17 km farther north into Carson Sink (Fig. 1). None of these investigations entailed a comprehensive study of the distribution, amount, and style of surface offsets for the July–August earthquake sequence. For these reasons, we conducted a detailed field survey of the 6 July and 23 August 1954 earthquake rupture zones to document the full extent and style of surface offsets, as well as the paleoseismic histories of the faults.

Methods

Structural and geomorphic details of the 6 July–23 August earthquake ruptures were mapped in the field on low-sun-angle aerial photographs taken in 1968, 1979, and 1990 at scales of 1:10,000 to 1:40,000. Conventional Army Map Service (AMS) photographs flown in 1957 (Nevada Bureau of Mines and Geology photo collection) were used to map details of surface ruptures in the northern part of the Carson Sink that are no longer preserved. Field observations compiled on 1:24,000-scale base maps were reduced to the 1:54,000-scale annotated maps included in this article (Fig. 2a–d). Because there are no significant field observations for the concealed ruptures north of Stillwater Reservoir (Fig. 2a), a detailed map is not provided for this area.

About 50 measurements of surface offset were acquired in the field and are annotated on Figure 2. Most measurements are of vertical separation of the ground surface. Measurements were all taken on gently sloping (<5°) to horizontal ground surfaces so the vertical separations closely approximate or equal the true vertical offset (i.e., throw) across the fault ruptures (e.g., Caskey, 1995). Vertical separation measurements account for ground-surface warping and multiple fault traces, which are common along the rupture trace. Right-laterally offset ephemeral stream channels were also observed locally and measured. The offset measurements are summarized in the slip distribution plot for the rupture zone (Fig. 3) along with Tocher's (1956) original measurements of vertical offset for comparison.

Two exploratory trenches were excavated along the southern part of the Rainbow Mountain fault to investigate its paleoseismic history. Detailed logs of these trenches and a field log of a natural exposure in Fourmile Flat are shown in Figures 6, 7, and 10. These logs, together with other field observations, form the basis for later discussion of the paleoseismic characteristics of the rupture zone.

Surface Rupture Characteristics

Distribution and Patterns of Historic Faulting

The 6 July and 23 August 1954 Rainbow Mountain rupture zone can be divided into three sections based on fault trace geometry and location: (1) a relatively linear, discontinuous zone of ruptures along the Rainbow Mountain fault, which extends northward into the Carson Sink; (2) a broad, discontinuous, northeast-trending zone of ruptures in the northern part of the Carson Sink; and (3) surface ruptures in Fourmile Flat. Additionally, minor reactivation occurred along the West Stillwater Range fault evidenced by small graben and fissures in the piedmont areas near Cox and Lambing canyons (Fig. 1). Each of the main rupture sections are described below and followed by a brief discussion of how the distribution of ground ruptures relate temporally to the sequence of events.

Rainbow Mountain Fault Ruptures. Surface ruptures along the east flank of Rainbow Mountain form a linear, north-northeast-trending, discontinuous zone extending northward from U.S. Highway 50 for a distance of 11 km along the eastern side of Rainbow Mountain and then for another 25 km northward into the Carson Sink (Figs. 1, 2a and b).

South of Stillwater Point Reservoir (Fig. 2a) where surface ruptures are generally well preserved, the rupture zone varies from a single fault trace to multiple overlapping strands reaching a maximum width of 2 km in the area just south of the reservoir. Surface breaks generally range in length from less than 100 m up to about 2 km. The longest continuous rupture extends from the northeastern side of Rainbow Mountain northward to the southern end of the Carson Sink for a distance of about 4 km (Fig. 2a). Several sections of the rupture trace south of the reservoir are marked by distinct left-stepping *en echelon* patterns (Fig. 2a). Of particular note, a 3-km-long north-trending zone of west-facing and left-stepping *en echelon* scarps defines the eastern
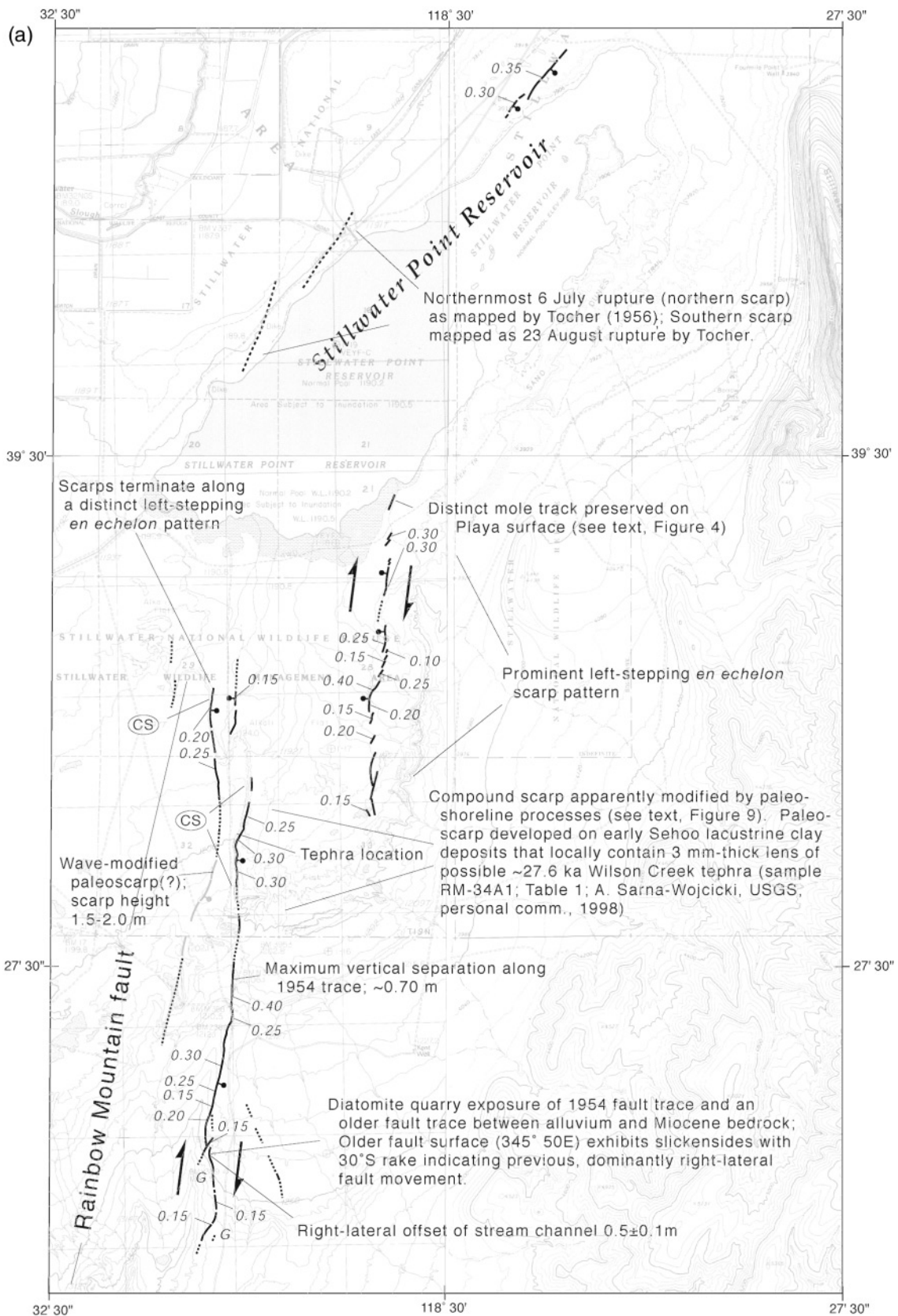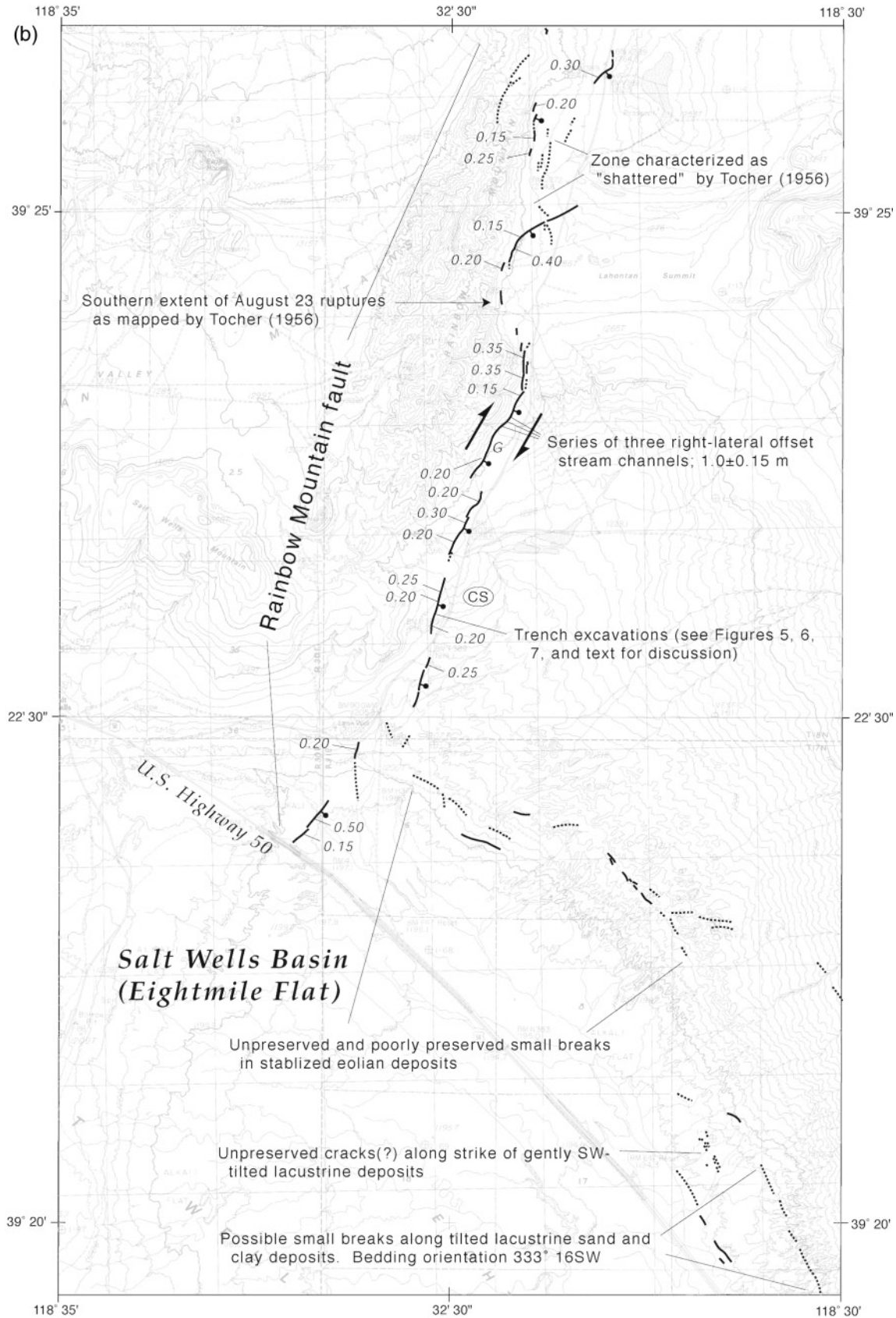
Figure 2.   Caption on page 6.
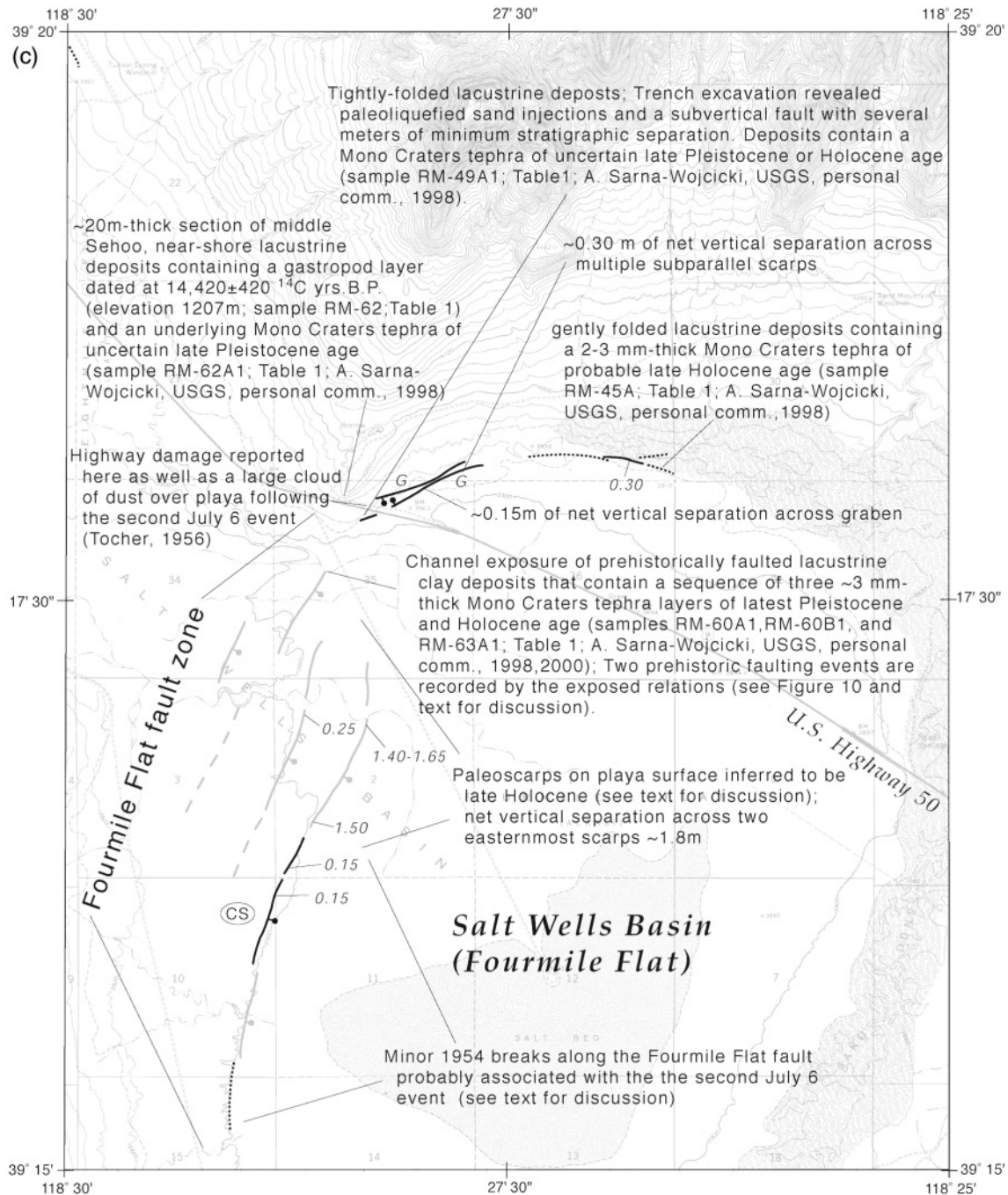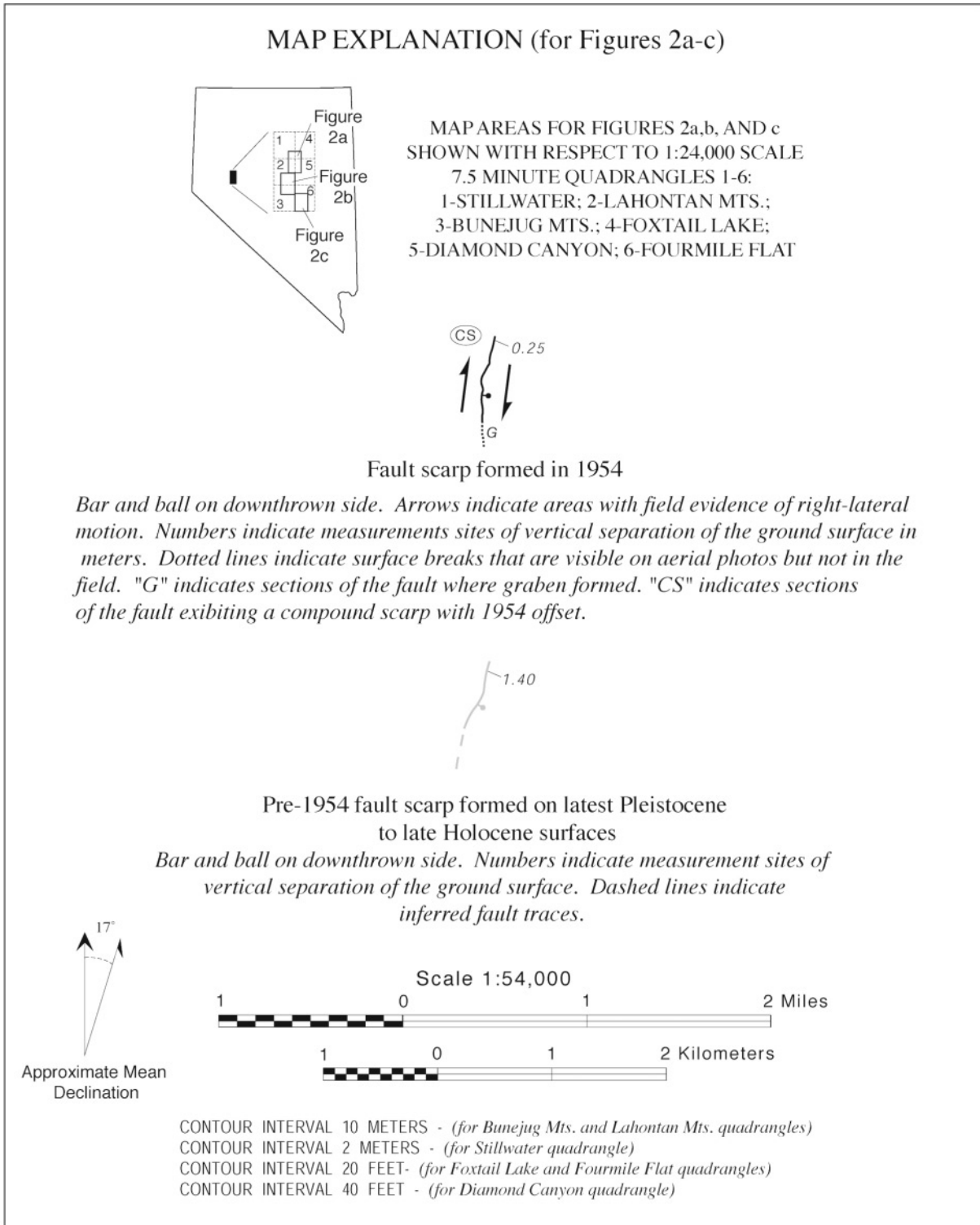
Figure 2.   Caption on page 6.

Figure 2.   Maps of fault scarps. (a) Fault scarps formed during the 6 July and 23 August 1954 Rainbow Mountain–Stillwater earthquake sequence. (b) Fault scarps formed during the 6 July and 23 August 1954 Rainbow Mountain–Stillwater earthquake sequence. (c) Fault scarps formed during the 6 July Fourmile Flat earthquake. See Figures 1 and 2d for figure locations. (d) Map explanation (on facing page). Source: S. John Caskey, John W. Bell, Alan R. Ramelli, and Steven G. Wesnousky.

side of a 1.5-km-wide graben in the area just south of the reservoir. The zone of west-facing scarps was previously unmapped and consists of numerous short (100- to 400-m-long) breaks, which terminate to the north along a distinct 200-m-long mole track (Fig. 4) that is still well preserved on the playa surface.

North of Stillwater Point Reservoir surface ruptures are no longer preserved because of the incohesive nature of surficial deposits and because this part of the basin has intermittently been inundated since the earthquakes. In our compilation (Fig. 1), we relied on existing, smaller-scale maps for this part of the rupture zone (Tocher, 1956; Slemmons,

(d)

MAP EXPLANATION (for Figures 2a-c)

MAP AREAS FOR FIGURES 2a,b, AND c
SHOWN WITH RESPECT TO 1:24,000 SCALE
7.5 MINUTE QUADRANGLES 1-6:
1-STILLWATER; 2-LAHONTAN MTS.;
3-BUNEJUG MTS.; 4-FOXTAIL LAKE;
5-DIAMOND CANYON; 6-FOURMILE FLAT

Figure 2a
Figure 2b
Figure 2c

(CS) 0.25
G

Fault scarp formed in 1954

Bar and ball on downthrown side. Arrows indicate areas with field evidence of right-lateral motion. Numbers indicate measurements sites of vertical separation of the ground surface in meters. Dotted lines indicate surface breaks that are visible on aerial photos but not in the field. "G" indicates sections of the fault where graben formed. "CS" indicates sections of the fault exibiting a compound scarp with 1954 offset.

1.40

Pre-1954 fault scarp formed on latest Pleistocene to late Holocene surfaces

Bar and ball on downthrown side. Numbers indicate measurement sites of vertical separation of the ground surface. Dashed lines indicate inferred fault traces.

17°

Scale 1:54,000

1   0   1   2 Miles

1   0   1   2 Kilometers

Approximate Mean Declination

CONTOUR INTERVAL 10 METERS - *(for Bunejug Mts. and Lahontan Mts. quadrangles)*
CONTOUR INTERVAL 2 METERS - *(for Stillwater quadrangle)*
CONTOUR INTERVAL 20 FEET- *(for Foxtail Lake and Fourmile Flat quadrangles)*
CONTOUR INTERVAL 40 FEET - *(for Diamond Canyon quadrangle)*

1957). In the Stillwater Marsh area, Tocher (1956) mapped two north-northeast-trending, east-facing scarps that extend north from the Stillwater Point Reservoir for a distance of about 17 km. The two fault traces overlap by about 2 km along a 1.5-km left step.

Northern Carson Sink Surface Ruptures. Surface breaks in the northern part of the Carson Sink consist of two distinct clusters (Fig. 1); a zone of dominantly northeast-trending scarps that lie on strike with the Rainbow Mountain fault ruptures to the south, and a less orderly complex of surface
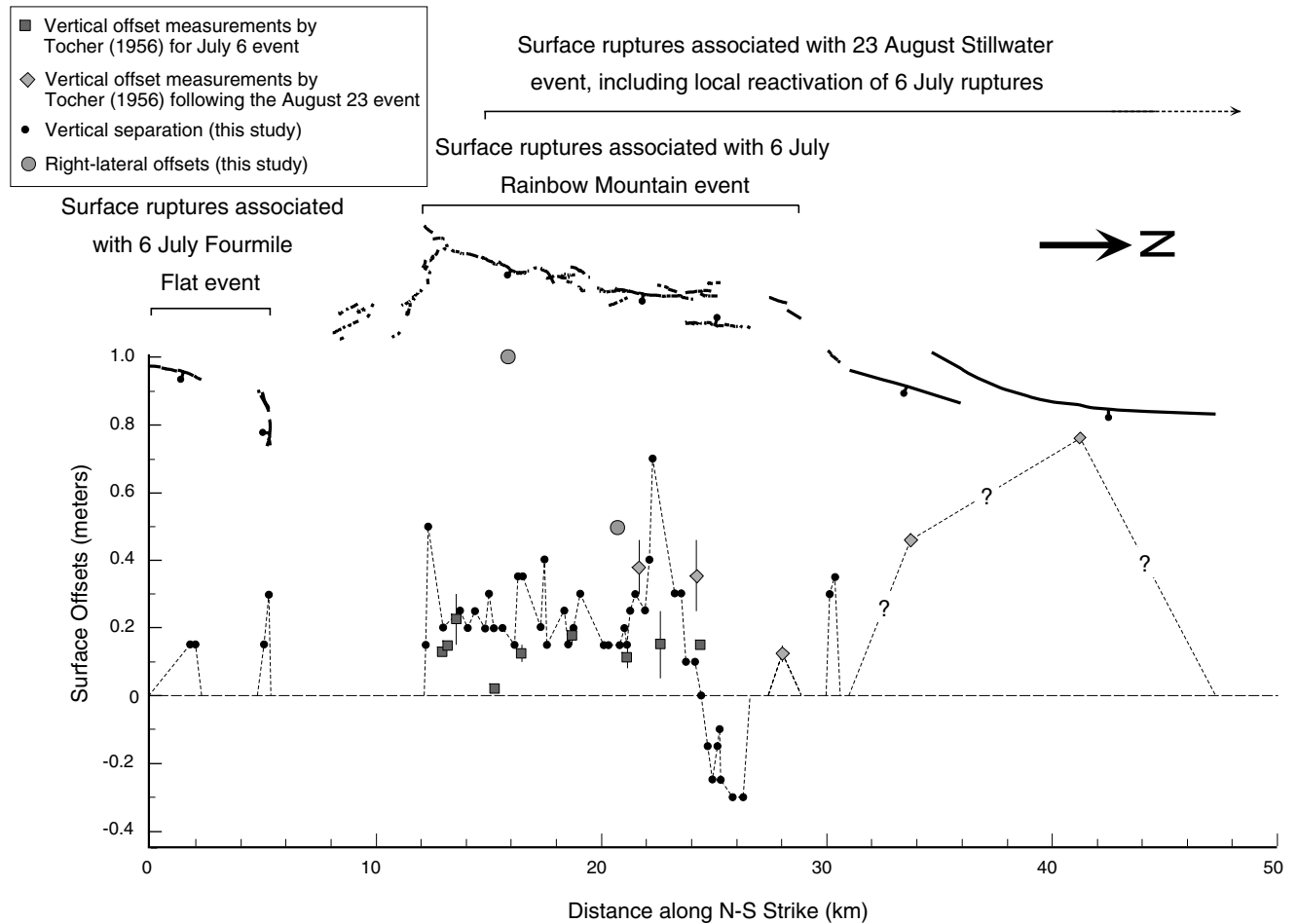
Figure 3.   Slip distribution for the Rainbow Mountain–Stillwater earthquake sequence showing measurements of vertical separation and right-lateral offset (this study) and vertical offset measurements made by Tocher (1956). Error bars on Tocher's measurements encompass the range of offsets reported at several closely spaced locations along the fault. Note that the right-lateral offset measurement at the 15-km mark represents several similar measurements on a series of three stream channels at that location. The 1954 rupture trace is shown above and registered to the slip distribution plot for reference. No displacement data are available for the ruptures that broke in the northern part of the Carson Sink (Fig. 1), so these ruptures are omitted for simplicity.

breaks located 10–20 km to the west. These ruptures are no longer preserved, so we have relied on the 1957 AMS aerial photos to map details of the surface breaks.

The zone of northeast-trending scarps comprises numerous, short (0.3- to 4.0-km-long) surface breaks that exhibit both down-to-the-east and down-to-the west sense of offset. The zone of ruptures is about 17 km long and broadens northward to maximum width of about 8 km. The zone is bounded to the southeast along a distinct linear alignment of northeast-trending surface breaks. The ruptures lie on strike with those to the south and tend to be well organized along northeast-trending patterns, suggesting they represent primary fault rupture. Conversely, we suspect that the less orderly complex of scarps located 10–20 km west are likely secondary ruptures related to ground shaking and/or liquefaction.

Salt Wells Basin Surface Ruptures.   Surface ruptures within Salt Wells Basin formed discontinuously along the northeastern rim of Eightmile Flat, the northern rim of Fourmile Flat and locally along the previously unmapped Fourmile Flat fault (Figs. 1, 2b and c).

An approximately 6-km-long zone of northwest-striking, discontinuous cracks and scarplets formed within eolian and lacustrine deposits along the northeast edge of Eightmile Flat playa (Tocher, 1956) (Fig. 2b). Aerial photo analysis and field observations in this area revealed numerous lineations defined by differential weathering of gently southwest-tilted lake beds found locally along this trend (Fig. 2b). It is uncertain whether the deformation of the lake deposits occurred in 1954.

The Fourmile Flat fault divides the Salt Wells Basin into Eightmile Flat to the west and the relatively down-dropped

Figure 4.   Photograph (view to the north) of a well-preserved mole track at the north end of a left-stepping en echelon alignment of west-facing scarps in the southern part of the Carson Sink (see Figs. 1 and 2a for location). The mole track indicates a large component of strike-slip offset along this section of the 1954 rupture trace. Stick is 1 m long.

Fourmile Flat to the east. The fault zone lies across a 10-km left step from the Rainbow Mountain fault to the northwest and is defined by a series of left-stepping *en echelon* paleoscarps that extend northward from the southern edge of the playa to the northern rim of Fourmile Flat playa. Small discontinuous 1954 breaks formed along the southern part of the easternmost strand of the Fourmile Flat fault (Fig. 2c) and also along the northeastern projection of the fault along the northern rim of the playa. The surface breaks along the northern rim of the playa locally form graben, which were interpreted by Tocher (1956) as secondary features related to ground shaking and possible liquefaction. However, the graben commonly exhibit small net vertical separations, suggesting they formed by actual vertical fault movements that are tectonic in origin. Additionally, the scarps along the playa rim appear to bend southward to merge with paleoscarps along the Fourmile Flat fault that are more clearly

tectonic in origin because they accommodate vertical displacements of the playa surface.

Similar to Eightmile Flat, lake deposits along the northern rim of Fourmile Flat are gently folded in the vicinity of 1954 surface breaks (Fig. 2c). It is unknown if the folding occurred in 1954. The lake deposits contain a late-Holocene tephra layer (Sample RM-45A; Table 1; A. Sarna-Wojcicki, U.S. Geological Survey [USGS], personal comm., 1998). About 100 m south of U.S. Highway 50, lacustrine deposits containing a latest Pleistocene or Holocene tephra layer (sample RM-49A; Table 1; A. Sarna-Wojcicki, USGS, personal comm., 1998) are more tightly folded, exhibiting moderate to steeply dipping beds in the location of a short 1954 surface break mapped by Tocher (1956). A backhoe excavation at this location showed the folded strata to be locally injected by liquefied sand and truncated by a subvertical fault with a minimum net stratigraphic separation of several meters (Fig. 2c), so it is clear that this area was affected by earlier (prehistoric) deformation.

Distribution of Fault Ruptures in Relation to the Sequence of Events

6 July Rainbow Mountain and 23 August Stillwater Earthquakes.   Tocher (1956) indicated that the 6 July Rainbow Mountain and 23 August Stillwater earthquakes both ruptured the Rainbow Mountain fault and northward into the Carson Sink. His mapping shows that the 23 August event ruptured primarily north of the 6 July ruptures, but it also partially reactivated and overlapped with the northern part of 6 July ruptures by approximately 12 km (Fig. 1). It is unknown if the newly mapped ruptures within the overlap zone and in the northern Carson Sink formed during the 6 July or the 23 August event. However, those in the northern Carson Sink likely represent the northern extent of the 23 August ruptures. This interpretation is most consistent with Tocher's (1956) observations and the more northerly epicentral location of the 23 August event relative to the 6 July events (Fig. 1; Doser, 1986).

Tocher (1956) indicated the 6 July Rainbow Mountain ruptures extend for a distance of 18 km, from U.S. Highway 50 north to the west side of Stillwater Point Reservoir (Fig. 2a). If the surface ruptures in the northern Carson Sink reflect primary rupture associated with the Stillwater earthquake, then the total rupture length of the Stillwater event is about 53 km (Table 2), from 6 km north of U.S. Highway 50 (i.e., Tocher's southern mapped extent of the 23 August ruptures [Fig. 2b]) to the northern Carson Sink. We consider this a minimum estimate because our measurements of surface offsets (Fig. 3) suggest that the 23 August reactivation of the 6 July ruptures along the Rainbow Mountain fault may have extended farther south than reported by Tocher (1956).

6 July Fourmile Flat Earthquake.   The 6 July Fourmile Flat earthquake occurred 11 hr after the mainshock. The Nevada Highway Patrol reported that U.S. Highway 50 was

Table 1

Radiocarbon Age and Tephra Data for the Rainbow Mountain Area

Field Sample Number	GX#*	Delta ^{13}C, ‰	Age (^{14}C years B.P.)	Calibrated Age ± 1σ (cal. B.P.)[†]	Material Sampled (unit)
RM-1	27178	−2.1	30,140 ± 1090	na	tufa (Qsg$_{1c}$, Fig. 6a).
RM-2	27179-AMS[‡]	−19.5	11,810 ± 50	$13,825^{+175}_{-190}$	bulk sample (Qsc, Fig. 6a)
RM-4	27180-AMS	−17.1	1730 ± 40	1567–1705	detrital charcoal (Qf$_{2/3}$, Fig. 6a)
RM-6	27181-AMS	−21.2	8060 ± 70	9008^{+21}_{-196}	detrital charcoal (Qf$_2$, Fig. 6b)
RM-7	27182-AMS	−23.4	14,550 ± 60	$17,423^{+265}_{-251}$	bulk sample from buried root zone (Qf$_1$, Fig. 6b)
RM-8	27252-AMS	−29.4	17,790 ± 70	$21,152^{+339}_{-331}$	bulk sample from buried root zone (Qf$_1$, Fig. 6a)
RM-11	27682-AMS	−20.9	6340 ± 40	7266^{+43}_{-17}	bulk sample from organic-rich sediment (Qf$_{2a}$, Fig. 6a)
RM-12	28206	+2.7	17,980 ± 270	$21,370^{+457}_{-447}$	ostracods (Qf$_{2a}$, Fig. 6b)
RM-13	28207	+3.1	18,200 ± 200	$21,624^{+409}_{-399}$	ostracods (Qf$_{2a}$, Fig. 5)
RM-14	81208-AMS	−25	9950 ± 60	11,232–11,549	detrital charcoal (Qf$_{2a}$, Fig. 6b)
RM-62	24186	−0.2	14,420 ± 420	$17,274^{+548}_{-536}$	gastropods (mid-Sehoo sand, Fig. 2c)
FM-1	29812	0.0	8850 ± 80	7787–8240	ostracods (late-Sehoo clay, Fig. 10)

Tephra Field Sample Number[§]	Source	Age (^{14}C years B.P.)	Calibrated Age ± 1σ (cal. B.P.)[†]	Unit Sampled and Comments
RM-34A1	Mono Craters	~27,600 (interpolated)	~32,800	early-Sehoo clay (Figure 2a)
RM-45A	Mono Craters	500–1500	524–1388	late-Holocene lacustrine deposits (Fig. 2c)
RM-49A1	Mono Craters	uncertain; but latest Pleistocene or Holocene	—	Sehoo lacustrine deposits
RM-60A1	Mono Craters	Holocene; <8850 ± 80	<7787–8240	late-Sehoo lacustrine clay (Fig. 2c); stratigraphically overlies FM-1 (this Table)
RM-60B1	Mono Craters	14,760 (interpolated)	~17,665	late-Sehoo lacustrine clay (Fig. 2c); correlates to RM-63A1
RM-62A1	Mono Craters	uncertain, but >14,420 ± 420	$>17,274^{+548}_{-536}$	mid-Sehoo(?) lacustrine deposits (Fig. 2c); stratigraphicaly underlies RM-62 (this Table)
RM-63A1	Mono Craters	14,760 (interpolated)	~17,665	mid-Sehoo lacustrine clay (Fig. 2c); correlates to RM-60B1

*All GX#'s refer to Geochron Laboratories sample numbers except for sample RM-14, which is a Lawrence Livermore National Laboratory sample number.

[†]Calibrated ages from Stuiver and Reimer (1993); range in calibrated ages given where multiple ages are determined from calibration curves.

[‡]AMS refers to samples analyzed by accelerator mass spectrometry.

[§]Tephra correlations and age estimations are from A. Sarna-Wojcicki, USGS, personal comm., 1998, 2000.

Table 2

Summary of Surface Rupture Characteristics for Faults Activated during the 1954 Rainbow Mountain–Stillwater Earthquake Sequence

Fault (event)	Rupture Length (km)	Average Strike	Dip	VS$_{max}$ (m)	VS$_{avg}$ (m)	SS$_{max}$ (m)	SS$_{avg}$ (m)	u$_{max}$ (m)	u$_{avg}$ (m)	M_0^g (max) (x/10^{26} dyn cm)	M_w (max)
Rainbow Mountain (6 July Rainbow Mtn)	18.0	017°	60°E	0.35 (?)	0.22 (?)	?	?	0.40 (?)	?	0.299	6.3
Fourmile Flat (6 July Fourmile Flat)	6.5	014°	70°E	0.30	0.22 (?)	0.00	0.00	0.35	?	0.095	6.0
Rainbow Mountain (23 August Stillwater)	53.0	017°	50°E	0.80	0.22 (?)	1.00 (?)	?	1.04	?	2.590	6.9
Additive totals for all three events										2.984	7.0

Abbreviations: VS$_{max}$ (maximum vertical separation of the ground surface) is taken to approximate maximum vertical displacement (throw); VS$_{avg}$ (average vertical separation) approximates average throw; SS$_{avg}$ (average lateral offset); SS$_{max}$ (maximum lateral offset); u$_{avg}$ (average surface displacement); u$_{max}$ (maximum surface displacement); M_0^g (max) (maximum geologic moment); M_w (max) (maximum moment magnitude). VS$_{max}$ values for the Rainbow Mountain and Stillwater ruptures reflect our measurements on strands attributed to each of the two events by Tocher (1956). VS$_{avg}$ value given for all three events reflects the average value of our vertical separation measurements for all strands shown on Figure 3. This VS$_{avg}$ value does not reflect vertical movements along the entire rupture zone because no displacement data are available for the northern 22 km of the rupture trace. We do not know whether SS$_{max}$ (1.00 m) occurred during the Rainbow Mountain or Stillwater event. For simplicity, we have used only the VS$_{max}$ values which are adjusted to dip-slip offsets for moment calculations. U$_{max}$ is calculated from dip slip (DS = VS/sinθ), where VS is vertical separation and θ is fault dip). Fault dip of 60° for the Rainbow Mountain fault is consistent with average field measurements of dip in exposures. Fault dips of 60° and 50° are used for the Fourmile Flat and Stillwater events, respectively, which are consistent with source parameters given by Doser (1986). M_0^g (max) for each fault ruptured were calculated from the relationship $M_0^g = \mu wLu$ (Aki and Richards, 1980), where μ is the shear modulus (3 × 10^{11} dyn/cm^2), w is fault width (assuming 12-km fault depths, which is consistent with the maximum focal depths given by Doser [1986], and adjusted for fault dip), L is end-to-end fault rupture length, and u is U$_{max}$. M_w (max) is calculated by the relation M_w = 2/3LogM_0^g−10.7 (Hanks and Kanamori, 1979) from the maximum geologic moments.

damaged during the large aftershock at 15:09 PDT (i.e., the Fourmile Flat earthquake) where surface ruptures along the northern rim of the Fourmile Flat playa crossed the road (Fig. 2c). Tocher (1956) noted that many people observed a large cloud of dust arising in the Fourmile Flat area at the time of the earthquake. Doser's (1986) relocation of this event lies in the southeast corner of Fourmile Flat (Fig. 1). Although this relocation has large uncertainties, the general location and anecdotal information indicate that the small 1954 scarps along the Fourmile Flat fault (Fig. 2c) probably formed during this event. We believe that the earthquake occurred on the Fourmile Flat fault and that the north-striking 1954 breaks along the southern portion of the fault represent primary surface rupture associated with this large aftershock. If we include the scarps along the north rim of Fourmile Flat with the 1954 ruptures along the fault to the south, then the end-to-end surface rupture length for the Fourmile Flat earthquake is 6.5 km (Table 2).

Style and Amount of Offset

Vertical separation measurements average about 0.22 m along the Rainbow Mountain fault ruptures with a maximum of 0.80 m (Fig. 3). Vertical separation along the Fourmile Flat fault ruptures ranges from 0.15 m to 0.30 m. We found evidence for right-lateral offsets locally along the 1954 rupture trace. In particular, right-lateral offsets between 0.50 and 1.00 m of several wash channels occur along the east side of Rainbow Mountain (Fig. 3). Coupled with prominent left-stepping *en echelon* scarp patterns along parts of the rupture zone (Fig. 2) and the distinct mole track on the Carson Sink playa, these offsets indicate that the earthquakes produced significant right-lateral movement. This is consistent with focal plane solutions for the three events (Doser, 1986), but contrasts with the findings of Tocher (1956) who reported no evidence for horizontal displacements.

The southern extent of the Stillwater event ruptures indicated by Tocher (1956) lies at about the 18-km mark on the slip distribution plot (Fig. 3). Our measurements of vertical separation are significantly larger between the 14- and 18-km marks than those made by Tocher (1956) along the 6 July ruptures. These larger measurements indicate that either: (1) reactivated slip during the 23 August event extended as much as 4 km farther south than recognized by Tocher; or (2) significant postseismic slip occurred along this part of the rupture. Because this section of the fault shows the largest right-lateral offsets, it is unknown which of the two events, or both, produced the offset.

Paleoseismicity along the Rainbow Mountain and Fourmile Flat Faults

The rupture trace in the Rainbow Mountain–Fourmile Flat area lies entirely below the latest Pleistocene highstand of pluvial Lake Lahontan (e.g., Morrison, 1964). Landscape modification associated with shoreline processes, fluctuating lake levels, and subsequent playa deflation have therefore obscured the tectonic geomorphology and evidence for pre-historic fault activity. However, modified paleoscarps are preserved along several sections of the Rainbow Mountain fault, including a section at the southern end of the Carson Sink (Fig. 2a) and another section approximately 3 km north of U.S. Highway 50 (Fig. 2b). Holocene paleoscarps are also well preserved along the Fourmile Flat fault (Fig. 2c).

Rainbow Mountain Fault

Two trenches across the 1954 Rainbow Mountain fault rupture expose offset lacustrine and subaerial deposits that record fluctuating levels during the most recent major lacustral cycle of Lake Lahontan. The Sehoo lake cycle, as termed by Morrison (1964), began at 25–30 ka with the rise of the early-Sehoo lake (Morrison, 1991). The early-Sehoo lake had receded nearly completely by about 15 ka and then rose rapidly to a highstand elevation of ~1332 m during mid-Sehoo time at ~13 ka (Broecker and Kaufman, 1965; Benson and Thompson, 1987; Morrison, 1991; Adams and Wesnousky, 1998). Following the mid-Sehoo highstand, the lake receded rapidly to near desiccation level and then fluctuated during smaller Holocene lacustral phases in late-Sehoo (i.e., mid-Holocene) and Fallon (i.e., late-Holocene) time.

The Rainbow Mountain trenches are located within an area of erosional shorelines and constructional beach bars at an elevation of 1228 m (Fig. 5). Located well below the 1332-m mid-Sehoo highstand, these well-preserved shoreline features record recession of the lake after 13 ka. The principal post-highstand shorelines defined by Morrison (1991) include the recessional S_2 (dendritic) shoreline at 1270 m and a late-Sehoo S_3 shoreline at approximately 1228 m (Morrison, 1964). The S_2 shoreline has been radiocarbon dated at about 11 ka (Broecker and Kaufman, 1965), and the S_3 shoreline was estimated to be 8–9 ka by Morrison (1991).

The low-sun-angle aerial photography (Fig. 5) and our field investigations reveal important cross-cutting relations between the fault scarp and shorelines at this site. An older, higher set of recessional strandlines are cut both by a paleoscarp and by the 1954 rupture, whereas a younger, lower constructional S_3 beach gravel bar truncates the paleoscarp and is offset only by the 1954 rupture. The cross-cutting relations therefore record an earthquake that postdates the S_2 stand and predates the S_3 gravel bar.

North Trench. The North trench was excavated across the paleoscarp, exposing a sequence of lacustrine and subaerial deposits that exhibit evidence for two pre-1954 faulting events (Fig. 2a).

North Trench Stratigraphy. The footwall of the fault is composed primarily of tuffaceous sandstone and mudstone of the Tertiary Truckee Formation (Ts) (Morrison, 1964), which at this location has been extensively eroded by shoreline processes and is overlain by a thin mantle of late Pleistocene and Holocene deposits.

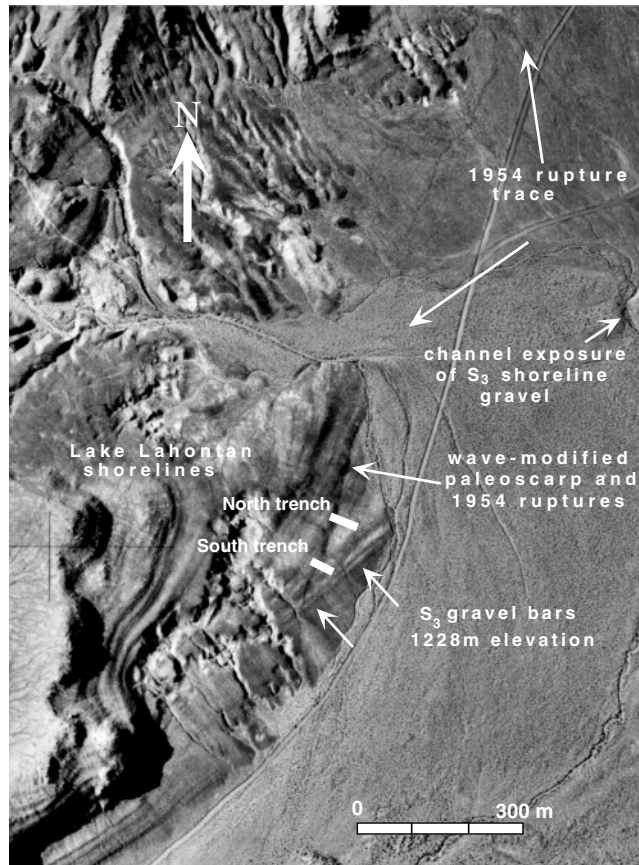The lowest unit in the hanging wall (Qf_1) is a poorly

Figure 5. Low-sun-angle photograph along the southern portion of the Rainbow Mountain fault in the vicinity of the Rainbow Mountain North and South trench sites (Figs. 6a and 6b). The North trench was excavated across a wave-modified paleoscarp. The S_3 shoreline gravel bars near the South trench (Morrison, 1991) (elevation 1228 m) clearly truncate the paleoscarp expressed at the North trench, but are broken by 1954 fault ruptures which are expressed as thin, crisp, dark lines. Channel exposure at S_3 shoreline is the location for radiocarbon samples RM-11 and RM-13 (see text, Table 1).

sorted, angular pebble sand consisting of locally derived clasts. The poorly sorted, angular clasts and a buried soil with a paleoroot zone in the top of Qf_1 indicate this unit was deposited in a subaerial, alluvial-fan environment. The paleoroot horizon yielded a radiocarbon age of 17.8 ka (Table 1; sample RM-8) indicating Qf_1 represents a subaerial period predating the mid-Sehoo lake phase.

Qf_1 is disconformably overlain by a sequence of mid-Sehoo beach deposits (Qsg_{1a-c}). The lowest unit of the sequence (Qsg_{1a}) consists of interbedded lacustrine beach sand and gravel; sand grades laterally (to the east) into horizontally bedded, sandy, rounded, pebble beach gravel. Units Qsg_{1b} and Qsg_{1c} consist of sandy pebble to cobble beach gravel, similar to Qsg_{1a}, but contain inclined layering and clast imbrication characteristic of deposition along a beach barrier. Qsg_{1b} contains locally prominent, eastward- (lake-

ward-) inclined clast imbrications representing beach barrier frontsets, whereas Qsg_{1c} contains prominent, westward- (landward-) inclined imbrications and layering characteristic of prograding beach-bar foresets. Calcareous tufa collected from Qsg_{1c} gravel yielded a radiocarbon age of 30.1 ka (Table 1; sample RM-1), which is anomalously old based on the underlying radiocarbon age of Qf_1 and known lake history, a relation we attribute to contamination by older, inherited carbonate.

Lower and upper beach gravels (Qsg_{1b-c} and Qsg_2) are separated by Qsc, a distinctive red-brown, 15-cm-thick clayey mud layer. Qsc likely represents offshore deposition during a period when the site was submerged by the mid-Sehoo lake. The reddish mud of Qsc impregnates and forms the matrix of most of Qsg_{1c}, the upper part of Qsg_{1b} in the central part of the trench, and the entire thickness of Qsg_{1b} gravel near the fault and in the footwall. Organic material in a bulk sample of Qsc yielded a radiocarbon age of 11.8 ka (Table 1; sample RM-2).
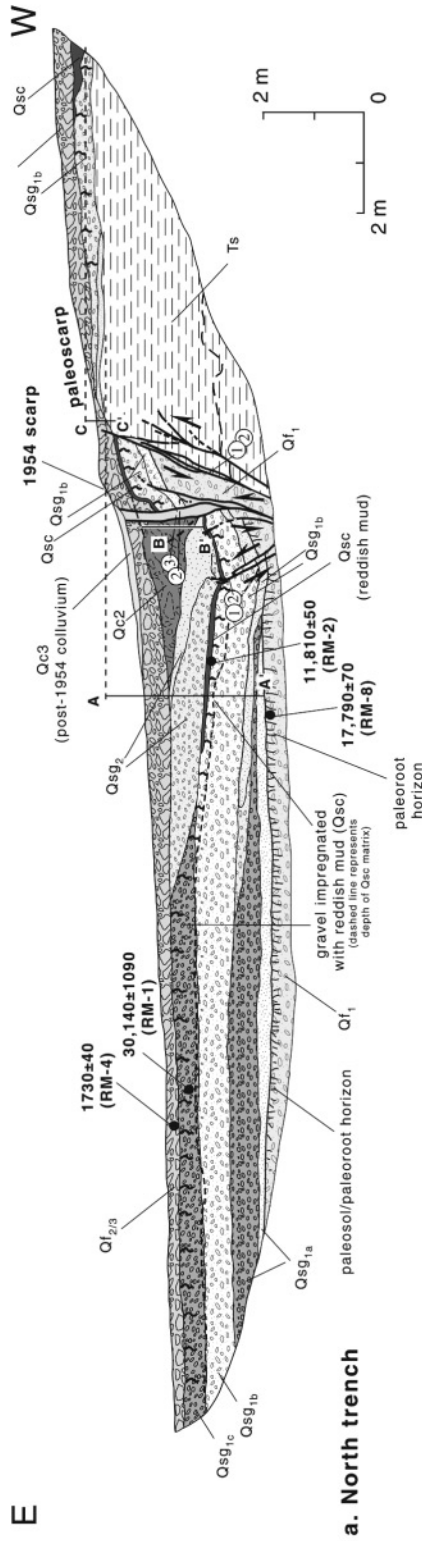
Qsc is overlain by beach gravel foresets of unit Qsg_2 likely deposited during the recessional phase that followed the S_2 (1270-m) lake stand. A 1-m-thick colluvial wedge (Qc_2), which is likely associated with the 1-m-high paleoscarp, in turn overlies unit Qsg_2.

Subaerial deposits ($Qf_{2/3}$) occur on the footwall where they overlie Qsc and a thin layer of Qsg_{1b} sand and gravel. The footwall surface is characterized by a moderately developed soil containing 10-cm-thick Av, 20-cm-thick Bw, and 35-cm-thick stage I–II Bk horizons. The hanging wall is also capped by a thin veneer of $Qf_{2/3}$ gravel that thickens to about 0.7 m near the scarp and may, in part, grade into the uppermost Qc_2 wedge deposits. A near-surface charcoal sample from $Qf_{2/3}$ yielded a radiocarbon age of 1.7 ka (Table 1; sample RM-4).

Adjacent to the fault zone, $Qf_{2/3}$ is overlain by a thin, colluvial-wedge deposit (Qc_3) associated with the 1954 rupture.

North Trench Structural Relations. The North trench exposes evidence of the three most recent earthquake ruptures, including the 1954 event (Figs. 6a and 7). The small historic fault scarp at the trench indicates that the 1954 earthquake produced only about 0.3 m of vertical offset at this location. The cumulative minimum vertical separation during the three events is estimated from 3.0 m of apparent minimum vertical offset of the top of Qf_1 deposits in the North trench (A–A', Fig. 6a).

Qsc (i.e., the reddish mud layer described above) forms a distinct marker bed that is also located within the fault zone and the western end of the footwall. Qsc is offset vertically by about 1.8 m (B–B' plus C–C', Fig. 6a), which represents the combined offset of the 1954 event and the penultimate, or second most recent event. Subtracting the 1954 offset indicates the penultimate event caused about 1.5 m of apparent vertical offset. This estimate is supported by the 1-m-thick colluvial wedge (Qc_2) because the thick-
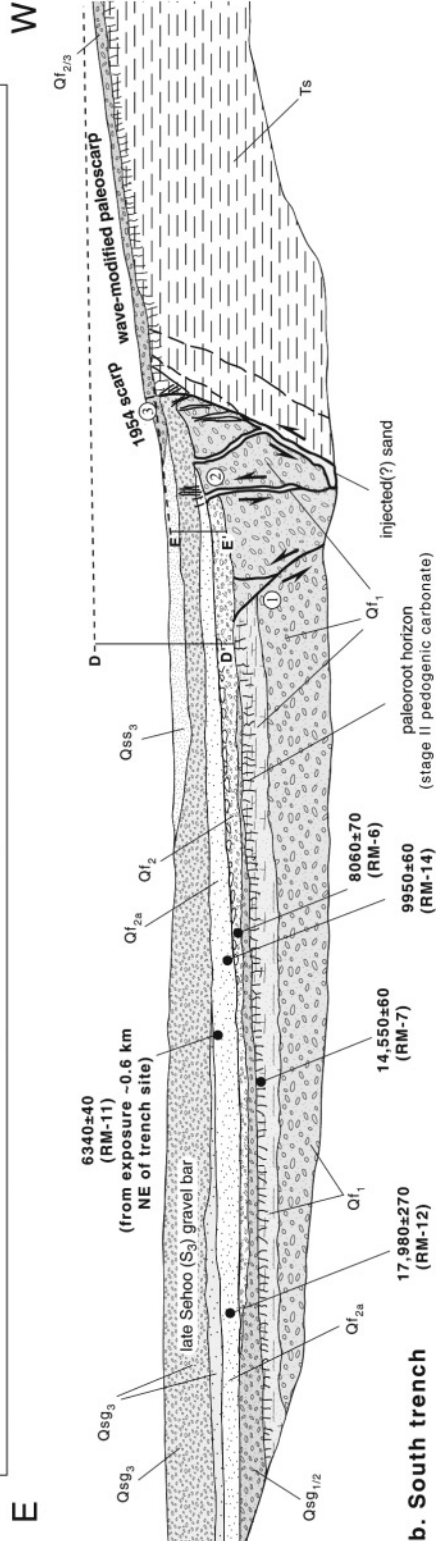
Figure 6. Simplified trench logs for Rainbow Mountain exploratory trenches: (a) North trench and (b) South trench. See Figures 1, 2b, and 5 for trench locations and text for discussion of the stratigraphic and structural relations expressed in the trench exposures. See Figure 7 for an enlarged log of the North trench fault zone. Circled numbers 1, 2, and 3 denote structural relations associated with the triultimate, penultimate, and 1954 events, respectively. Black markings at the top of Qsg_{1c} and Qsg_{1b} and below Qsc denote the upper limit of reddish (Qsc) mud-impregnated beach gravel.

STRATIGRAPHIC UNITS

Qc_3 - post-1954 colluvium
Qf_3 - post late-Sehoo subaerial deposits (post-6.3 ka)
Qss_3 - late-Sehoo to recent sand deposited behind Qsg_3 (~6.3 ka)
Qsg_3 - late-Sehoo lacustrine beach barrier sand and gravel (~6.3 ka)
$Qf_{2/3}$ - subaerial deposits of post mid-Sehoo and/or post late-Sehoo age
Qc_2 - post penultimate-event colluvium (post–8.1–9.9 ka, pre–6.3 ka)
Qf_{2a} - post mid-Sehoo ostracod-bearing subaerial(?) deposits (6.3–9.9 ka)
Qf_2 - post mid-Sehoo subaerial deposits (~8.1–9.9 ka)
$Qsg_{1/2}$ - mid-Sehoo lacustrine sand and gravel corr. to Qsg_2 or Qsg_1 in north trench
Qsg_2 - mid-Sehoo lacustrine sand and gravel (<11.8 ka)

Qsc - mid-Sehoo lacustrine red clayey mud (11.8 ka)
$Qsg_{1/2}$ - mid-Sehoo lacustrine sand and gravel corr. to Qsg_2 or Qsg_1 in north trench
Qsg_2 - mid-Sehoo lacustrine sand and gravel (<11.8 ka)
Qsc - mid-Sehoo lacustrine red clayey mud (11.8 ka)
Qsg_{1c} - mid-Sehoo lacustrine sand and gravel (11.8–14.5 ka)
Qsg_{1b} - "
Qsg_{1a} - "
Qf_1 - pre mid-Sehoo subaerial deposits (>14.5–17.8 ka)
Ts - Tertiary Truckee Formation (Morrison, 1964)

①②③ - Denotes structural relations associated with the
triultimate ①, penultimate ②, and 1954 ③ events.
(see text for discussion)

a. North trench

W

E

Qsc
Qsg_{1b}
2 m
2 m
0
Ts
1954 scarp
paleoscarp
C
C'
①②
Qf_1
Qc_3
(post-1954 colluvium)
Qsc Qsg_{1b}
Qsc Qsg_{1b}
B
②③
B'
Qsg_{1b}
Qsc
(reddish mud)
Qsg_2
Qc_2
A
A'
①②
11,810±50
(RM-2)
17,790±70
(RM-8)
gravel impregnated
with reddish mud (Qsc)
(dashed line represents
depth of Qsc matrix)
paleoroot
horizon
Qf_1
1730±40
(RM-4)
30,140±1090
(RM-1)
$Qf_{2/3}$
paleosol/paleoroot horizon
Qf_2
Qsg_{1a}
Qsg_{1c} Qsg_{1b}

b. South trench

W

E

$Qf_{2/3}$
Ts
1954 scarp
wave-modified paleoscarp
③
②
①
Qf_1
injected(?) sand
paleoroot horizon
(stage II pedogenic carbonate)
D
D'
E
E'
Qss_3
Qf_2
Qf_{2a}
8060±70
(RM-6)
9950±60
(RM-14)
14,550±60
(RM-7)
Qf_1
6340±40
(RM-11)
(from exposure ~0.6 km
NE of trench site)
late Sehoo (S_3) gravel bar
17,980±270
(RM-12)
Qf_{2a}
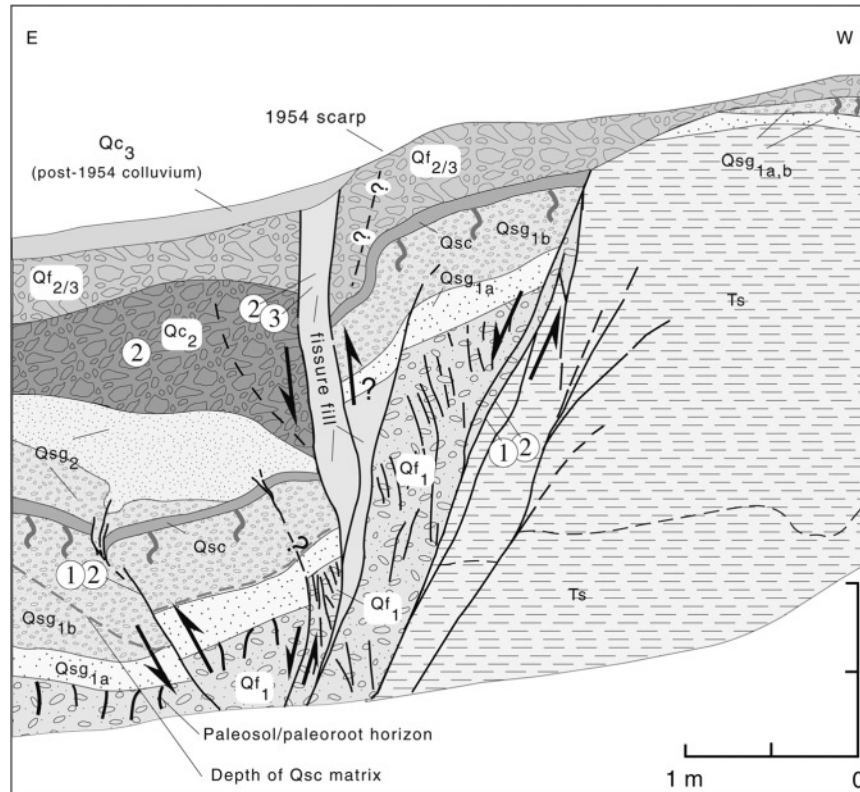Qsg_3
Qsg_3
$Qsg_{1/2}$
Qf_1
Qf_2

1267

Figure 7.   Enlarged log for the fault zone area of the North trench (Fig. 6a). Stratigraphic units and event numbers correspond to those in Figure 6a.

ness of colluvial wedges must be less than or equal to the associated vertical offset.

Qsg_1 and the upper Qf_1 deposits containing the paleosol are offset in an apparent reverse sense across a steeply west-dipping fault strand located 1 m east of the main fault zone. This reverse fault does not offset Qsc in a reverse sense, although it may have been reactivated during a subsequent event as an extensional structure evidenced by the minor normal offset and fissuring of Qsc near the tip of the reverse fault strand. Because the apparent reverse fault displaces only Qsg_1 and older units, it records the oldest identifiable event exposed in the trench (i.e., the triultimate, or third most recent event). Extensional reactivation of the reverse fault likely occurred during the penultimate event, which resulted in most of the displacement of Qsc.

Deformation during the 1954 event is associated with a 0.25-cm-thick sand- and gravel-filled fissure that bounds Qc_2 to west. 1954 deformation may also be associated with localized down-warping and folding of Qsg_1 and overlying units west of the fissure.

The main east-dipping fault strand that bounds Ts must have accommodated movement during the penultimate, triultimate, and perhaps earlier events, but this strand did not rupture at the surface during the 1954 event. Evidence for earlier, pretriultimate faulting are the pervasive fractures in Qf_1, which are not present in overlying units, and the sig-

nificant vertical displacement required by the position of the large fault-bounded block of Qf_1 within the fault zone. However, we have no timing or displacement constraints for discrete events involving the older Qf_1 deposits that underlie the paleosol.

South Trench.   The South trench (Fig. 6b) is at a slightly lower elevation than the North trench and crosses the 1954 rupture where the late-Sehoo lake phase associated with the S_3 shoreline largely eroded the paleoscarp visible at the North trench. The South trench exposed relations similar to the North trench, with the addition of deposits associated with the S_3 gravel bar. The South trench also records evidence for two pre-1954 earthquakes.

South Trench Stratigraphy.   Similar to the North trench, the footwall of the South trench is composed primarily of the Tertiary Truckee Formation (Morrison, 1964), which is overlain by a thin mantle of Holocene subaerial deposits ($Qf_{2/3}$).

The lowermost unit in the hanging wall of the South trench correlates to the mid-Sehoo subaerial deposit (Qf_1) exposed in the North trench. Here Qf_1 includes a lower section of angular, poorly sorted, alluvial gravel and an upper section of silt containing a soil and paleoroot horizon. The paleoroot horizon yielded a radiocarbon age of 14.6 ka (Table 1; sample RM-7), similar to the 17.8-ka age from the

North trench. The presence of Stage II + pedogenic carbonate in the buried soil suggests the Qf_1 deposits may be significantly older than the 14.6-ka soil age, which we interpret to approximate the age of subaerial exposure just prior to the mid-Sehoo transgression. Qf_1 is disconformably overlain by $Qsg_{1/2}$, which consists of a thin deposit of undifferentiated mid-Sehoo beach gravel. Correlation of $Qsg_{1/2}$ to Qsg_1 or Qsg_2 in the South trench is uncertain because $Qsg_{1/2}$ pinches out east of the fault zone and it is unclear whether $Qsg_{1/2}$ pre- or post-dates earlier movement on the fault.

Qf_1 and $Qsg_{1/2}$ are disconformably overlain by a 10-cm-thick layer of predominantly poorly sorted, angular Qf_2 alluvial-fan gravels and reworked rounded beach cobbles. Detrital charcoal from Qf_2 yielded a radiocarbon age of 8.1 ka (Table 1; sample RM-6). Qf_{2a} consists of subaerial(?) sand composed of abundant ∼1-mm-diameter ostracod shells. Detrital charcoal from the base of Qf_{2a} yielded a radiocarbon age of 10.0 ka (Table 1; sample RM-14). Hence, the ages of Qf_2 and of Qf_{2a} are stratigraphically inverted.

Qf_{2a} is overlain by as much as 1 m of late-Sehoo beach-barrier gravel (Qsg_3) and sand (Qss_3) that represent the S_3 shoreline identified elsewhere by Morrison (1964). Qsg_3 consists of pebble–cobble gravel with locally prominent eastward-inclined clast imbrications in the eastern part of the trench and prominent westward-inclined imbrications and layering in the western part, representing beach-barrier frontsets and foresets, respectively. The S_3 beach barrier is geomorphically well preserved (Fig. 5) and clearly truncates the paleoscarp present at the North trench.

S_3 shoreline gravel is also present about 600 m northeast of the trench sites (Fig. 5). A channel cut at this location exposes beach gravel overlying an organic-rich sandy mud that yielded a radiocarbon age of 6.3 ka (Table 1; sample RM-11). An ostracod-rich sand similar to unit Qf_{2a} in the South trench lies below the 6.3-ka mud horizon. Shells from the sand in the channel cut and from the south trench yielded nearly identical radiocarbon ages of 17.9 and 18.2 ka, respectively (Table 1; samples RM-12, RM-13). Because these ages are older than several ages from stratigraphically lower or equivalent units, we believe the ostracod shells were reworked from older lacustrine deposits and were likely emplaced by eolian processes during the subaerial period preceding the late-Sehoo lacustral phase. In addition, the ostracods vary in the degree of preservation and consist of a mix of species that inhabited differing water salinities (R. Forester, USGS, personal comm., 2002), which supports the interpretation that the ostracods were reworked from older deposits.

South Trench Structural Relations.   Similar to the North trench, the South trench exposes evidence for three earthquake events. In the South trench, Qsg_3 gravel is offset only by the 1954 break that splays upward from the main east-dipping fault. Qsg_3 clearly postdates older west-dipping and subvertical strands of the fault zone related to earlier events. The 1954 vertical offset is similar to that at the North trench (about 0.3 m). The minimum vertical separation of

the top of Qf_1 for the three events (2.8 m) is similar to that in the North trench and is estimated by the vertical distance between the top of Qf_1 in the footwall and the down-slope projection of the upper surface from the top of the paleoscarp (D–D′, Fig. 6b).

Qf_2 is truncated by a subvertical fault trace that exhibits a few centimeters of sandy fissure fill and at least 15 cm of vertical separation of the top of Qf_1. This fault trace is in turn truncated by Qf_{2a} and therefore records the penultimate event. If Qf_2 correlates to $Qf_{2/3}$ gravel capping the footwall, then the gravel unit is vertically offset by about 1.2 m (E–E′, Fig. 6b), which is less than the 1.8 m of combined historic and penultimate offset of Qsc observed in the North trench. The inverted radiocarbon ages from Qf_2 and Qf_{2a} (8.1–10.0 ka) are problematic because these two units appear to bracket movement on the subvertical, penultimate fault stand. For simplicity, we use both of these ages to approximate the lower age limit for the penultimate event.

Similar to the North trench, an easternmost fault strand dips west and displaces Qf_1 in an apparent reverse sense. Within the fault zone, the upper silty alluvium and paleoroot horizon of Qf_1 are missing, suggesting they were uplifted and eroded from the west side of the reverse fault prior to deposition of Qf_2. The reverse fault is truncated by Qf_2, which is in turn truncated by a fault strand associated with the penultimate event. Therefore we interpret the apparent reverse fault in the South trench to have also formed during the triultimate faulting event.

The lower part of the main east-dipping fault zone is filled by a 20-cm-thick, well-sorted, medium-grained sand. The clean texture of the deposit differs markedly from all units exposed along the fault. We suspect that the sand was emplaced by injection related to liquefaction, indicating that either the lake level or groundwater table were close to the trench elevation during at least one of the paleo-events. The lack of shear fabric in the sand suggests that it was injected during the more recent, penultimate event.

Summary of Lacustral and Subaerial Deposition.   The oldest Quaternary unit exposed in the trenches (alluvial-fan gravel Qf_1) was deposited subaerially during the desiccation phase separating the early- and mid-Sehoo lake phases (Morrison, 1991); radiocarbon ages of 17.8 and 14.6 ka from Qf_1 estimate the age of the desiccation phase. The lowermost beach sand and gravel (Qsg_{1a} in the North trench) represents the onset of the transgressive mid-Sehoo lacustral phase (after 14.6 ka). The rising lake went through at least minor fluctuations, producing the succession of Qsg_{1a-c} beach sand and gravel.

Following deposition of the Qsg_{1c} gravel-bar deposits, the lake rose to the maximum mid-Sehoo highstand at an elevation of 1332 m (∼13 ka). During this time the trench sites were submerged. As the lake level fell to the S_2 recessional shoreline (1270 m), the offshore mud (Qsc) was deposited (∼11.8 ka).

During the post-S_2 recessional phase, the lake level

dropped to the North trench elevation where shoreline Qsg_2 gravels were deposited and then dropped below the trench site to near desiccation level (Morrison, 1991). At this time subaerial alluvial-fan gravel and eolian sand (Qf_2 and Qf_{2a} in South trench) were deposited (8.1–10.0 ka). Only minor Qsg_1 and/or Qsg_2 lacustrine deposits are present in the South trench, suggesting that erosion of these units occurred prior to deposition of Qf_2, probably during the post-S_2 recessional phase.

During late-Sehoo time, the lake rose during the last major lacustral (S_3) phase to the elevation of the South trench (1228 m); our radiocarbon ages suggest this phase took place after 8–10 ka, and possibly after 6.3 ka. This latter age suggests a significantly younger age for the S_3 stand than Morrison's (1991) estimate of 8–9 ka, although the 6.3-ka age would place the S_3 stand within the Altithermal, a period generally accepted to be warmer and drier than normal. Finally, the lake again receded to near desiccation level, and late-Holocene Qf_3 alluvial-fan gravel was deposited at the site.

Event Timing and Slip Rate Estimates for the Rainbow Mountain Fault.   Based on structural–stratigraphic relations, two pre-1954 faulting events are recognized in both trenches (Figs. 5 and 6). The older of the two events (i.e., triultimate event) offsets Qf_1 and lower Qsg_1 deposits, but does not offset Qsc. The event age is constrained between 11.8 and 14.6–17.8 ka (Fig. 8). In the North trench, the penultimate event displaces Qsc lake mud and Qsg_2 sand and gravel, and in the South trench the event displaces Qf_2 deposits, but it does not displace overlying Qsg_3. The age of the penultimate event lies between 6.3 ka and 8.1–10.0 ka.

The cumulative vertical separation during the three events is estimated from 3.0 m of apparent minimum vertical offset of Qf_1 deposits in the North trench and 2.8 m in the South trench. Approximately 0.3 m of the 3.0-m net vertical offset is accounted for by the 1954 event. Net vertical separation of Qsc across the two main fault traces in the North trench is estimated to be 1.8 m. Subtracting the 0.3 m of 1954 vertical offset provides an estimate of the vertical separation during the penultimate event (1.5 m). Hence, the triultimate and penultimate events show about 1.2 m (min-

imum) and 1.5 m of apparent vertical offset, respectively. The apparent vertical offset of ~3.0 m averaged over the past 14.6–17.8 ka suggests a vertical slip rate of 0.17–0.21 mm/yr.

A component of lateral slip during the triultimate and penultimate events is suggested by the apparent reverse offsets. A quarry across the fault ~13 km north of the trench sites revealed slickensides with a rake angle of 30°S on a pre-1954 strand of the fault oriented 345°50E (Fig. 2a). A slip azimuth of 325° determined from the fault and slickenside measurements and rake angle are similar to those determined instrumentally for the Rainbow Mountain and Stillwater events (326° and 340°; 40°S and 35°S, respectively; Doser, 1986). If we infer a similar net slip azimuth (325°) at the trench sites, where the fault strikes 015° and dips 65°E, this equates to a right-oblique slip rate of 0.20–0.25 mm/yr. Alternatively, if we assume that a 30°S rake angle (rather than a 325° slip azimuth) characterizes the net slip direction, this results in a significantly larger right-oblique slip rate of 0.37–0.46 mm/yr.

Relationships along Paleoscarps at the North End of Rainbow Mountain

Three north-trending, left-stepping escarpments are present between Rainbow Mountain and the Stillwater Point Reservoir. The scarps average about 1.5 km long, are as much as 5.0 m high, and scarp crests lie at elevations of about 1200 m. Small (<0.25-m-high) scarps formed in 1954 along the base of nearly the entire lengths of the two southernmost escarpments (Fig. 9). In this area, the 1954 rupture trace closely parallels the curvatures of the receded scarp crest, which clearly indicates that the 5-m-high escarpment is a prehistoric fault scarp. The fault scarp formed on thinly laminated, early-Sehoo lacustrine clay that locally contains a 1- to 2-mm tephra layer which likely correlates to the 27.6-ka Wilson Creek Bed 15 (Table 1; sample RM-34A1; A. Sarna-Wojcicki, USGS, personal comm., 1998). The gentle (<15°) scarp slopes in this area indicate that the scarps have undergone significant fault-parallel erosional retreat (Fig. 9), but little scarp-derived colluvium is present. This relation suggests the scarps may have been modified by shoreline
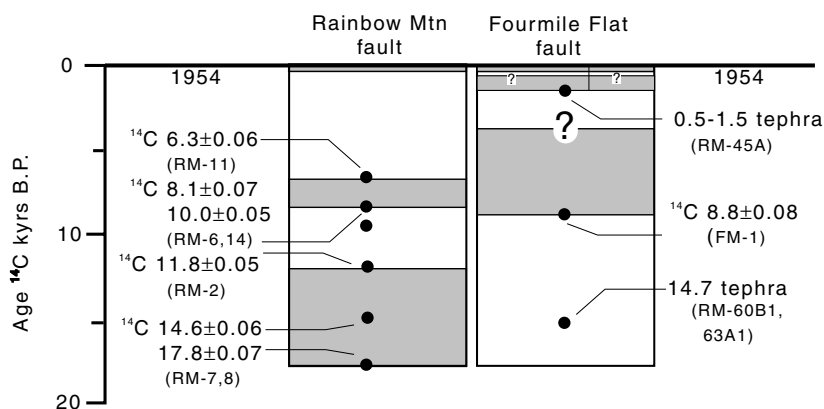

Figure 8.   Event diagram for the Rainbow Mountain and Fourmile Flat faults based on age constraints from exploratory trench exposures across the Rainbow Mountain fault (Fig. 6), a natural exposure in Fourmile Flat (Fig. 10), and regional stratigraphic relations. Bracketed time intervals for events are shown in gray. Ages are uncalibrated ^{14}C k.y. B.P. Radiocarbon and tephra samples (in parentheses) are listed in Table 1.
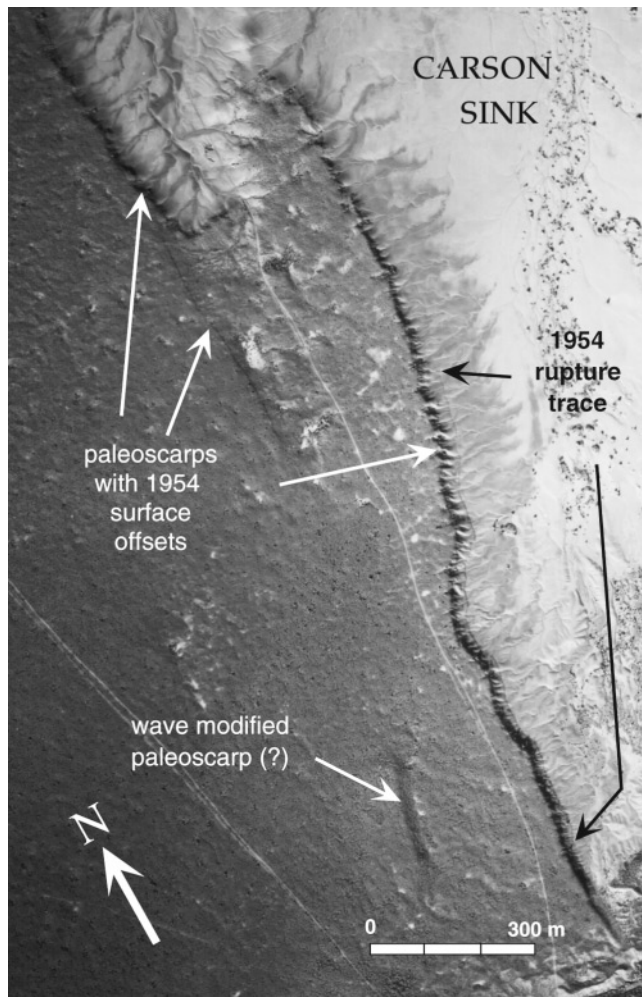
Figure 9. Low-sun-angle photograph circa 1968 showing small 1954 scarps (~25 cm high) along the base of a ~5-m-high paleoscarp near the southern part of the Carson Sink. The paleoscarps are developed on early-Sehoo Lake Lahontan lacustrine clay containing a tephra layer (Table 1; sample RM-34 A1) which best correlates with Wilson Creek bed 15 dated at ~31.9–27.6 k.y. B.P. (A. Sarna-Wojcicki, USGS, personal comm., 1998). See Figures 1 and 2a for location and text for discussion.

processes of mid- or late-Sehoo lacustral phases that washed scarp-derived detritus into the Carson Sink. The structural and stratigraphic relations require at least one prehistoric faulting event on this part of the Rainbow Mountain fault since 27.6 ka. An upper age limit to the paleoscarps is also poorly constrained because modification of the scarps may have occurred during mid- or late-Sehoo time (13–6 ka), or perhaps during more recent lake levels that reached elevations of ~1200 m or greater.

Fourmile Flat Fault Zone

Stratigraphic Relations. A natural channel cut that crosses a strand of the Fourmile Flat fault 0.5 km south of U.S High-

way 50 (Fig. 2c) exposes mid-Sehoo lacustrine clay deposits that record latest Pleistocene and Holocene offsets (Fig. 10). Although parts of the Fourmile Flat fault ruptured at the surface in 1954, there is no evidence for historic rupturing along the section of the fault exposed in the channel cut. The channel cut exposes a 15-m-wide fault zone that disrupts a 2-m-thick section of olive-brown lacustrine clay deposits that contain three tephra layers, each being about 2–3 mm thick. The lowermost tephra (T1) (Table 1; samples RM-60B1 and RM-63A1) best correlates with the Wilson Creek ash bed #4 dated at 14.7 [14]C k.y. B.P. (A. Sarna-Wojcicki, USGS, personal comm., 1998, 2000), consistent with the clay being a deep-water, mid-Sehoo lacustrine deposit. The two upper tephra (T2 and T3) form a couplet separated stratigraphically by about 10 cm. Tephra T3 (Table 1; sample RM-60A1) is similar to several mid- to late-Holocene tephra from Mono Craters in eastern California (A. Sarna-Wojcicki, USGS, personal comm., 1998), so we are not able to definitively determine its age. However, osctracods collected from directly beneath the T2/T3 tephra couplet yielded an age of 8.8 ka (Table 1; sample FM-1), which is consistent with the 14.7-ka age for the lower tephra layer and a mid-Holocene age for the tephra couplet.

Sequence of Events. Tephra layer T1 is offset vertically approximately 1.8 m across the fault zone, whereas the playa surface is offset vertically by only 0.6 m. Tephra layers T2 and T3 are not exposed on the west side of the fault zone. We interpret these relations to require: (1) an earliest (triultimate) faulting event that produced a 1.2-m vertical offset of the 14.7-ka T1 tephra and the younger (post–8.8-ka) strata containing the tephra couplet (T2 and T3); (2) erosional leveling of the playa surface (e.g., deflation)—enough to remove the pre-existing 1.2-m-high scarp and uplifted strata containing the tephra couplet on the west side of the fault; (3) a second (penultimate) faulting event responsible for forming the present 0.6-m-high paleoscarp. Other playa paleoscarps up to 1.5 m high are preserved along other strands of the fault zone to the south (Fig. 2c). These paleoscarps are interpreted to have also formed during the penultimate event; and (4) localized reactivation along the Fourmile Flat fault zone north and south of the exposure during the second 6 July earthquake.

The maximum limiting age for the triultimate event on the Fourmile Flat fault is provided by the 8.8-ka ostracods sampled from just below the T2/T3 tephra couplet. Scarps formed during the triultimate event have been completely eroded with no discernible scarp-derived colluvium or younger lake deposits present on the down-dropped, east side of the fault (Fig. 10). These relations require significant deflation (i.e., greater than 1 m) of the playa surface and imply that the triultimate event probably occurred prior to nearly complete dessication of Lake Lahontan. It is unknown whether Lake Lahontan completely dessicated prior to the ~6.3-ka (?) S$_3$ lake level rise.

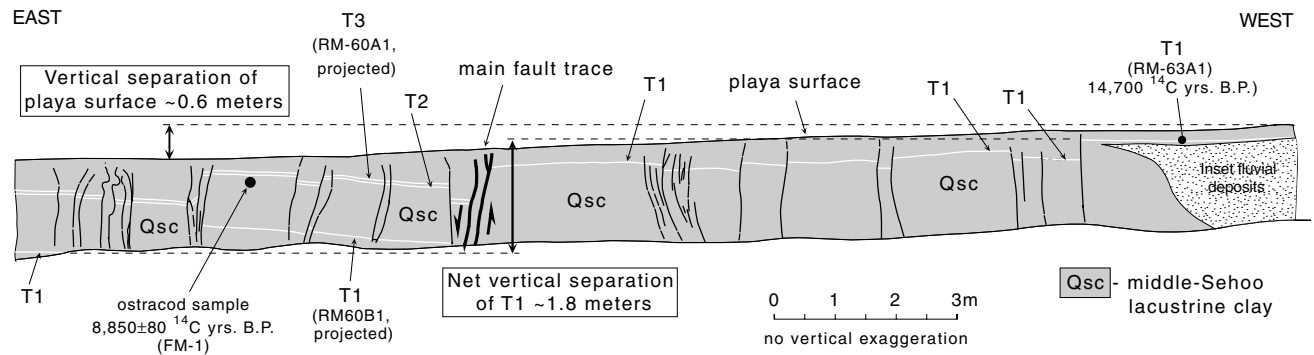A maximum limiting age for the penultimate event is

Figure 10.   Log of channel exposure across a strand of the Fourmile Flat fault (see Fig. 2c for location). The exposure reveals evidence for two prehistoric events (see text for discussion). Minor historic fault scarps mapped north and south of this exposure (Fig. 2c) likely formed during the 6 July 1954 Fourmile Flat earthquake. However, no 1954 offsets are evident at this location. Three separate tephra layers of Mono Craters affinity (Table 1; A. Sarna-Wojcicki, USGS, personal comm., 1998, 2000) are shown as thin white layers. Tephra T1 is vertically separated by ~1.8 m across the fault, whereas the scarp on the playa surface is only 0.6 m high, indicating evidence for two pre-1954 surface rupturing events on the fault at this location.

estimated by age of the S_3 shoreline (~6.3 ka) determined at the Rainbow Mountain trench sites. The well-preserved paleoscarps in Fourmile Flat lie well below the 1228-m elevation of the S_3 shoreline, and we consider it unlikely that the scarps produced by the penultimate event pre-date the late-Sehoo lake stand. The presence of deformed late-Holocene strata along the north rim of Fourmile Flat suggest a much younger age for the penultimate event. In this area, north-tilted and gently folded lacustrine strata contain a tephra that best correlates to a late-Holocene Mono Craters tephra (Table 1; sample RM-45A; Fig. 2c). It is unlikely that the lake beds were deformed during the 1954 earthquake, which produced only minor 1954 surface breaks in this area. We therefore interpret that the lake beds were deformed during the penultimate event, and that the event occurred in the late Holocene. Late-Holocene Mono Craters tephra in this region have been dated by radiocarbon ages of associated deposits between 500 and 1500 yr B.P. (Davis, 1978; Bell, unpublished data). A late-Holocene age for the penultimate Fourmile Flat fault scarps is consistent with their youthful geomorphic expression, especially considering the scarps are developed on poorly consolidated lacustrine clay deposits. We therefore infer that the age of the penultimate event on the Fourmile Flat fault occurred after 500–1500 yr B.P. We can constrain the upper age limit to the triultimate event as only pre-penultimate event (i.e., prior to 500–1500 yr B.P.).

Slip Rates.   Slip rate estimates for the Fourmile Flat fault are not straightforward because we have limited knowledge about the amount of net offset across the zone during the triultimate event as well as the amount of long-term lateral offset. We consider the ~1.2 m of vertical offset recorded in the exposure for the triultimate event to be a minimum for the fault zone as a whole. All of the paleoscarps developed on the playa surface to the south have similar geo-

morphic expression and most likely formed during the penultimate event (i.e., after erosional beveling of the playa surface) because prexisting scarps would likely have been removed or severely degraded by the S_3 lake. Just south of the channel exposure, net vertical separation across two paleoscarps that overlap along-strike is about 1.8 m (Fig. 2c). The 1954 vertical surface offsets across the zone are localized and reach a maximum of only 0.15 m along the central portion of the fault zone. Not including the localized historic offsets, the total net vertical offset across the zone is then roughly 3.0 m over the past 8.8 ka, yielding a minimum vertical slip rate estimate of 0.34 mm/yr. We have no geologic data concerning a long-term lateral component of slip or fault dip at depth. However, the left-stepping scarp geometry and strong right-lateral component of slip determined from the focal mechanism for the Fourmile Flat event (Doser, 1986) suggests that the lateral slip component along the fault is similar to that along the Rainbow Mountain fault. If we infer Doser's (1986) instrumentally determined fault dip and slip azimuth for the Fourmile Flat earthquake (70°E and 331°, respectively) to the long-term slip along the ~010°-striking fault, we estimate a post–8.8-ka right-oblique slip rate of ~0.40 mm/yr for the Fourmile Flat fault.

Discussion

Comparison of Paleoseismic Event Chronologies and Slip Rates for the Rainbow Mountain and Fourmile Flat Faults

The Rainbow Mountain and Fourmile Flat faults form an *en echelon* left-stepping pattern and both ruptured with right-oblique slip during the 1954 earthquake sequence (Doser, 1986). Although both faults show evidence for three post ~14-ka surface rupturing events, including the 1954

earthquakes, the faults have different slip rates and earthquake histories (Fig. 8). The age of the triultimate event is poorly constrained for the Fourmile Flat fault at post-8.8 ka and prior to erosional beveling of the playa, the timing of which is unknown. The triultimate event on the Rainbow Mountain fault (14.6–11.8 ka) does not coincide with a recognizable event on the Fourmile Flat fault. Age constraints for the penultimate event on the Rainbow Mountain fault (10.0–6.3 ka) overlap with constraints for the triultimate event on the Fourmile Flat faults, so it is conceivable that these events may have occurred close in time, similar to the 1954 sequence. The penultimate event on the Fourmile Flat fault is required to postdate the 1228-m Lake Lahontan (S_3) shoreline but probably occurred in the late Holocene (post–500–1500 yr B.P.), so this event does not overlap with events recognized along the Rainbow Mountain fault. It's important to note that the 1954 vertical displacements are much smaller in comparison to those associated with the two prehistoric events recorded for both faults.

The estimated Holocene oblique slip rate for the Fourmile Flat fault (0.40 mm/yr) is similar to the larger estimate for the post-latest Pleistocene oblique slip rate for the Rainbow Mountain fault (0.20–0.46 mm/yr) even though the Fourmile Flat fault length (10 km) is only a fraction of the overall length of the Rainbow Mountain fault (60 km). The significant slip rate and average recurrence rate (~3 ka) for the relatively short Fourmile Flat fault indicates that it is an important component of an active system of faults accommodating oblique, northwest-oriented extension in the region (Thatcher *et al.*, 1999; Caskey and Bell, 2001), and that even minor active faults can be important for characterizing regional strain rates and patterns.

Comparisons of Geologic, Seismological, and Geodetic Data for the 1954 Rupture Zone

Geologic, seismological, and geodetic studies of the Rainbow Mountain–Stillwater earthquake sequence indicate right-normal-oblique displacements on east-dipping faults (Doser, 1986; Hodgkinson *et al.*, 1996), although the geologic evidence for right-lateral motion is only locally expressed along the historic rupture trace. Hodgkinson *et al.* (1996) reanalyzed geodetic data sets of Whitten (1957) and modeled horizontal and vertical displacements of 0.9 m and 0.2 m, respectively, for the Rainbow Mountain–Stillwater sequence, which are essentially identical to field measurements presented here (Table 2).

Geologically determined moment magnitudes based on fault rupture length and displacement are in agreement with those determined instrumentally only if we use the maximum vertical separation measurements in our calculations (Table 3). We do not assign the relatively large (1.0-m) strike-slip offsets to either the Rainbow Mountain or Stillwater events in our calculations because we are uncertain as to which earthquake to attribute these values. However, the 1.0 m of right-lateral offset is essentially equivalent to the 1 m of maximum surface displacement (i.e., dip-slip offset)

assigned to ruptures that broke during the Stillwater event (Table 2). It is possible that the use of maximum slip works better for moment calculations of these ruptures only because the large component of lateral slip determined from focal mechanisms (Doser, 1986) is underrepresented at the surface for all three events. Our moment magnitude calculations using maximum surface offsets for the Rainbow Mountain and Stillwater earthquakes (6.3 and 7.0, respectively) are identical to surface-wave magnitudes reported for the two events (Bonilla *et al.*, 1984) (Table 3). The moment magnitudes we calculate for both the Rainbow Mountain and Fourmile Flat event (6.3 and 6.0, respectively) are essentially equal to those determined by Doser (1986) from body-wave modeling (6.2 and 5.9). However, the M_w 7.0 we calculate for the Stillwater event is significantly larger than the M_w 6.5 moment magnitude determined by Doser (1986). The moment magnitudes determined from the new geologic data appear to resolve previous discrepancies between seismologically and geologically determined magnitudes, particularly between the surface wave magnitudes and those determined using the geologic data previously reported by Tocher (1956) (Table 3). This is particularly true for the Stillwater event since our mapping increased the rupture length of the earthquake by 22 km.

A significant discrepancy exists between the northwest strikes of the preferred first-motion nodal planes (Fig. 1) and body-wave models (Doser, 1986) and north- to northeast-strikes of the surface rupture zones for each of the three events. Interestingly, the nearby 1932 Cedar Mountain and 1954 Fairview Peak earthquakes also produced surface ruptures which showed a significantly more easterly strike than the first-motion nodal planes for the events (Doser, 1986; Caskey *et al.*, 1996; Bell *et al.*, 1999). In the Cedar Mountain area (Fig. 1, inset), these relations led previous workers (Gianella and Callaghan, 1934; Molinari, 1984; Bell *et al.*, 1999) to interpret the surface ruptures as being related to fault movement at depth in the fashion of Riedel shears (Fig. 11) (Riedel, 1929; Tchalenko, 1970; Wilcox *et al.*, 1973; Naylor *et al.*, 1986; Sylvester, 1988). We also suggest the discrepancy between seismologically determined fault-plane geometry and surface geology for these events might be explained this way.

The mismatch between fault geometry at depth and at the surface may be responsible for the discontinuous and somewhat distributed surface ruptures of the 1954 earthquake sequence and the apparent inefficient transfer of right slip to the surface during the Rainbow Mountain–Stillwater sequence. Nevertheless there is close agreement between the instrumentally derived slip azimuth and the geologically derived slip azimuths for the 1954 Fairview Peak ruptures, particularly where larger surface offsets occurred in the epicentral area (Caskey *et al.*, 1996). This relation also holds true for the Rainbow Mountain fault when the instrumental slip azimuths are compared to the net slip direction observed on a prehistoric strand of the fault.

Table 3

Comparison of Magnitudes Calculated for the 1954 Rainbow Mountain–Stillwater
Earthquake Sequence

Event	M*	M_o (wave form modeling; Doser [1986])[†]	M_s[‡]	M_o (geology; [Tocher 1956])[§]	M_o (geology; this study)[‖]
6 July Rainbow Mountain	6.6	6.2	6.3	6.0	6.3
6 July Four Mile Flat	6.4	5.9	—	—	6.0
23 August Stillwater	6.8	6.5	7.0	6.4	6.9

*Magnitudes of uncertain type given by Doser (1986).

[†]Moment magnitudes determined from teleseismic body wave modeling (Doser, 1986).

[‡]Surface wave magnitudes (Bonilla *et al.*, 1984).

[§]Moment magnitudes calculated by Doser (1986) using geological fault parameters of Tocher (1956).

[‖]Moment magnitudes calculated using field measurements of maximum vertical separation and other geological and seismological fault parameters (Table 2). Moment calculations from geologic data use the equations given in Table 2.
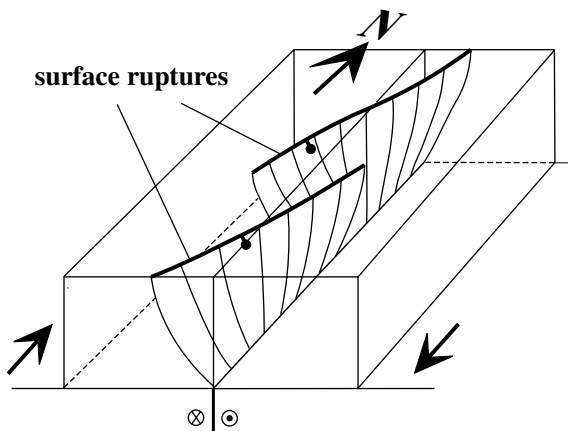
Figure 11. Three-dimensional model for ruptures of the 1954 earthquake sequence. The north–north-east-striking fault ruptures along the 1954 Rainbow Mountain–Stillwater–Fairview Peak earthquake sequence are all oblique to the north–northwest striking nodal planes for the events (Doser, 1986). The observations suggest that the fault ruptures may rotate clockwise and fan upward from fault ruptures at depth in the fashion of Riedel shears. Figure modified from Naylor *et al.* (1986).

Conclusions

New information on surface ruptures of the 6 July and 23 August 1954 Rainbow Mountain–Stillwater earthquake sequence reveals several previously unrecognized areas of historic faulting. These areas extend the rupture zone by 25 km to a total length of 70 km. Surface ruptures identified along the previously unrecognized Fourmile Flat fault, together with anecdotal evidence and event locations indicate that the triggered 6 July aftershock (i.e., the Fourmile Flat earthquake) produced minor, primary fault rupture. More than 50 field measurements of surface offset constrain the distribution of slip for the discontinuous and distributed fault ruptures. Of particular note, several measurements and indicators of lateral offset such as left-stepping *en echelon*

patterns and a well-preserved mole track provide evidence for a significant component of dextral shear for the events. Evidence of lateral offset was not previously reported for the sequence, but is consistent with seismologic and geodetic data (Doser, 1986; Hodgkinson *et al.*, 1996). Geologic moments calculated from our new data also agree with seismologically determined moments, if we use maximum surface offsets in our calculations.

The latest Pleistocene to recent paleoseismic histories for the Rainbow Mountain and Fourmile Flat faults are different although both faults have experienced three surface-rupturing events during the past ~15 ka including the 1954 earthquakes. Timing constraints on the triultimate events for the two faults do not overlap. However, constraints on the penultimate event on the Rainbow Mountain and triultimate event on the Fourmile Flat faults overlap and, conceivably, these events could have occurred close in time, similar to the 1954 sequence. The penultimate event along the southern part of the Rainbow Mountain fault pre-dates a late-Sehoo (S_3) Lahontan shoreline gravel bar formed at an elevation of 1228 m. A bulk radiocarbon date suggests that the S_3 shoreline gravel may be younger than 6.3 ka. The penultimate event along Fourmile Flat fault is required to have formed after the lake receded from the S_3 shoreline and probably occurred during the late Holocene. Estimated net slip rate for the Fourmile Flat fault (0.40 mm/yr) is similar to the Rainbow Mountain fault slip rate (0.20–0.46 mm/yr) even though the 10-km total length of the Fourmile Flat fault is only a fraction of the length of the Rainbow Mountain fault rupture zone (~60 km), indicating that even minor active faults can be important for characterizing regional strain rates and patterns.

References

Adams, K. A., and S. G. Wesnousky (1998). Shoreline processes and the age of the Lake Lahontan highstand in the Jessup embayment, *Geol. Soc. Am. Bull.* **110,** no. 6, 1318–1332.

Aki, K., and P. G. Richards (1980). *Quantitative Seismology: Theory and Methods*, W. H. Freeman, New York, 932 pp.

Beanland, S., and M. M. Clark (1994). The Owens Valley fault zone, eastern California, and surface faulting associated with the 1872 earthquake, *U.S. Geol. Surv. Bull. 1982*, 29 pp.

Bell, J. W. (1984). Quaternary fault map of Nevada, Reno Sheet, Nevada Bureau of Mines and Geology Map 79, Reno, scale 1:250,000.

Bell, J. W., C. M. de Polo, A. R. Ramelli, A. M. Sarna-Wojcicki, and C. E. Meyer (1999). Surface faulting and paleoseismicity of the 1932 Cedar Mountain earthquake area, west-central Nevada, and implications for modern tectonics of the Walker Lane, *Geol. Soc. Am. Bull.* **111,** no. 6, 791–807.

Benson, L. V., and R. S. Thomson (1987). Lake-level variation in the Lahontan basin for the past 50,000 years, *Quaternary Res.* **28,** 69–85.

Bonilla, M. G., R. K. Mark, and J. J. Lienkaemper (1984). Statistical relations among earthquake magnitude, surface rupture length, and surface displacement, *Bull. Seism. Soc. Am.* **74,** 2379–2411.

Broecker, W. S., and A. Kaufman. (1965). Radiocarbon chronology of Lake Lahontan and Lake Bonneville II, Great Basin, *Geol. Soc. Am. Bull.* **69,** 1009–1032.

Caskey, S. J. (1995). Geometric relations of dip slip to a faulted ground surface: new nomograms for estimating components of fault displacement, *J. Struct. Geol.* **17,** 1197–1202.

Caskey, S. J., and J. W. Bell (2001). Comparisons of historic fault slip motions and paleoseismic slip rates to the geodeticvelocity field across the central Nevada seismic belt in the vicinity of the 1954 earthquake sequence, *Seism. Res. Lett.* **72,** no. 2, 280–281.

Caskey, S. J., S. G. Wesnousky, P. Zhang, and D. B. Slemmons (1996). Surface faulting of the 1954 Fairview Peak (Ms 7.2) and Dixie Valley (Ms 6.8) earthquakes, central Nevada, *Bull. Seism. Soc. Am.* **86,** 761–787.

Davis, J. O. (1978). Quaternary tephrachronology of the Lake Lahontan area, Nevada and California, Nevada Archeological Survey Research Paper 7, University of Nevada, Reno, 137 pp.

Dohrenwend, J. C., B. A. Schell, C. M. Menges, B. C. Moring, and M. A. McKittrick (1996). Reconnaissance photogeologic map of young (Quaternary and late Tertiary) faults in Nevada, Nevada Bureau of Mines and Geology Open-File Report 96-2.

Doser, D. (1986). Earthquake processes in the Rainbow Mountain–Fairview Peak–Dixie Valley, Nevada region 1954–1959, *J. Geophys. Res.* **91,** 12,572–12,586.

Gianella, V. P., and E. Callaghan (1934). The Cedar Mountain, Nevada, earthquake of December 20, 1932, *Bull. Seism. Soc. Am.* **24,** 345–377.

Hanks, T. C., and H. Kanamori (1979). A moment magnitude scale, *J. Geophys. Res.* **84,** 2348–2350.

Hodgkinson, K. M., R. S. Stein, and G. Marshall (1996). Geometry of the 1954 Fairview Peak-Dixie Valley earthquake sequence from a joint inversion of leveling and triangulation data: *J. Geophys. Res.* **101**(B11), 25,437–25,457.

Molinari, M. P. (1984). Late Cenozoic geology and tectonics of Stewart and Monte-Cristo Valleys, west-central Nevada, *Master's Thesis*, University of Nevada, Reno.

Morrison, R. B. (1964). Lake Lahontan: geology of the southern Carson Desert, Nevada, *U.S. Geol. Surv. Profess. Pap. 401* 156 pp.

Morrison, R. B. (1991). Quaternary stratigraphic, hydrologic, and climatic history of the Great Basin, with emphasis on Lake Lahontan, Bonneville, and Tecopa, in *Quaternary Nonglacial Geology: Conterminous U.S.*, R. B. Morrison (Editor), *Geology of North America*, Vol. K-2, Geological Society of America, Boulder, Colorado, 283–320.

Naylor, M. A., G. Mandl, and C. H. K. Sijpesteijn (1986). Fault geometries in basement-induced wrench faulting under different initial stress states: *J. Struct. Geol.* **8,** 737–752.

Riedel, W. (1929). Zur Mechanik geologischer Brucherscheinungen, *Zbl. Mineral. Geol. Paläontol., Abt. B*, 354–368.

Slemmons, D. B. (1957). Geological effects of the Dixie Valley–Fairview Peak, Nevada, earthquakes of December 16, 1954, *Bull. Seism. Soc. Am.* **47,** 353–375.

Steinbrugge, K. V., and D. F. Moran (1956). Damage caused by the earthquakes of July 6 and August 23, 1954, *Bull. Seism. Soc. Am.* **46,** no. 1, 16–33.

Stewart, J. H. (1988). Tectonics of the Walker Lane belt, western Great Basin: Mesozoic and Cenozoic deformation in a zone of shear, in *Metamorphism and Crustal Evolution of the Western United States*, W. G. Ernst (Editor), Prentice Hall, Englewood Cliffs, New Jersey, 683–713.

Stewart, J. H., and J. E. Carlson (1978). Geologic map of Nevada, *U.S. Geol. Surv.* in cooperation with Nevada Bureau of Mines and Geology, scale 1:500,000.

Stuiver, M., and P. J. Reimer (1993). Extended 14C database and revised CALIB radiocarbon calibration program, *Radiocarbon* **35,** 215–230.

Sylvester, A. G. (1988). Strike-slip faults, *Geol. Soc. Am. Bull.* **100,** 1666–1703.

Tchalenko, J. S. (1970). Similarities between shear zones of different magnitudes, *Bull. Seism. Soc. Am.* **81,** 1625–1640.

Thatcher, W., G. R. Foulger, B. R. Julian, J. Svarc, E. Quilty, and G. W. Bawden (1999). Present-day deformation across the Basin and Range province, western United States, *Science* **283,** 1714–1718.

Tocher, D. (1956). Movement on the Rainbow Mountain fault, *Bull. Seism. Soc. Am.* **46,** no. 1, 10–14.

Wallace, R. E. (1984). Fault scarps formed during the earthquakes of October 2, 1915, in Pleasant Valley, Nevada, and some tectonic implications, *U.S. Geol. Surv. Prof. Pap. 1274-A*, 1–33.

Whitten, C. A. (1957). Geodetic measurements in the Dixie Valley area, *Bull. Seism. Soc. Am.* **84,** 974–1002.

Wilcox, R. E., T. P. Harding, and D. R. Seely (1973). Basic wrench tectonics, *Am. Assoc. Petr. Geol. Bull.* **57,** 74–96.

Department of Geosciences
San Francisco State University
1600 Holloway Avenue
San Francisco, California 94132
caskey@sfsu.edu
  (S.J.C.)

Nevada Bureau of Mines and Geology
University of Nevada
Reno, Nevada 95521
jbell@unr.edu
ramelli@unr.edu
  (J.W.B., A.R.R.)

Center for Neotectonic Studies
University of Nevada
Reno, Nevada 95521
stevew@seismo.unr.edu
  (S.G.W.)